nature cell biology

The EMT-activator Zeb1 is a key factor for cell plasticity and promotes metastasis in pancreatic cancer

Angela M. Krebs[1,2,3,4], Julia Mitschke[5], María Lasierra Losada[1], Otto Schmalhofer[5], Melanie Boerries[3,4,6], Hauke Busch[3,4,6], Martin Boettcher[7], Dimitrios Mougiakakos[7], Wilfried Reichardt[3,4,8], Peter Bronsert[3,4,9], Valerie G. Brunton[10], Christian Pilarsky[11], Thomas H. Winkler[12], Simone Brabletz[1], Marc P. Stemmler[1,13,14] and Thomas Brabletz[1,13,14]

Metastasis is the major cause of cancer-associated death. Partial activation of the epithelial-to-mesenchymal transition program (partial EMT) was considered a major driver of tumour progression from initiation to metastasis. However, the role of EMT in promoting metastasis has recently been challenged, in particular concerning effects of the Snail and Twist EMT transcription factors (EMT-TFs) in pancreatic cancer. In contrast, we show here that in the same pancreatic cancer model, driven by Pdx1-cre-mediated activation of mutant *Kras* and *p53* (KPC model), the EMT-TF Zeb1 is a key factor for the formation of precursor lesions, invasion and notably metastasis. Depletion of *Zeb1* suppresses stemness, colonization capacity and in particular phenotypic/metabolic plasticity of tumour cells, probably causing the observed *in vivo* effects. Accordingly, we conclude that different EMT-TFs have complementary subfunctions in driving pancreatic tumour metastasis. Therapeutic strategies should consider these potential specificities of EMT-TFs to target these factors simultaneously.

Metastasis is still the major cause of cancer-associated death. Partial activation of the embryonic epithelial-to-mesenchymal transition program (partial EMT) was considered a major driver of tumour progression from initiation to metastasis[1–3]. Most studies involved manipulation of different EMT-inducing transcription factors (EMT-TFs), such as Snail, Slug, Twist and ZEB1, in cell-culture or xenograft mouse models. In particular, the EMT-activator ZEB1 was shown to be important for tumorigenicity and metastasis, by triggering combined activation of cell motility and stemness properties[4–6]. However, the role of EMT in invasion and metastasis was challenged by two recent publications using genetic mouse models for breast and pancreatic cancer[7,8]. In particular, genetic depletion of the EMT-activators *Snai1* or *Twist1* had no effect on tumour initiation, invasion or metastasis in pancreatic cancer (PDAC) driven by Pdx1-cre-mediated activation of mutant *Kras* and *p53* (KPC model)[8]. Therefore the authors claimed that EMT is dispensable for metastasis.

We used here the same KPC mouse model for pancreatic cancer and conditionally ablated the EMT-activator *Zeb1* in tumour cells. In contrast to *Snai1* and *Twist1*, depletion of *Zeb1* strongly affected formation of precursor lesions, tumour grading, invasion and notably metastasis during PDAC progression. In summary, we conclude that EMT is important for metastasis, but there is considerable variability and tissue specificity (and not redundancy) in the role and function of different EMT-TFs.

RESULTS

Zeb1 depletion reduces grading, invasion and distant metastasis in PDAC

KPC mice develop metastatic pancreatic cancers with an almost 100% penetrance[9]. Of note, a fraction of cancer cells and cells in precursor lesions (PanINs) express the EMT-TF Zeb1. This was considered to be important for disease progression[10], which we

[1]Department of Experimental Medicine 1, Nikolaus-Fiebiger-Center for Molecular Medicine, FAU University Erlangen-Nürnberg, Glückstrasse 6, 91054 Erlangen, Germany. [2]University of Freiburg, Faculty of Biology, Schaenzlestrasse 1, 79104 Freiburg, Germany. [3]German Cancer Consortium (DKTK), 79106 Freiburg, Germany. [4]German Cancer Research Center (DKFZ), 69121 Heidelberg, Germany. [5]Department of General and Visceral Surgery, University of Freiburg Medical Center, Hugstetter Strasse 55, 79106 Freiburg, Germany. [6]Systems Biology of the Cellular Microenvironment Group, Institute of Molecular Medicine and Cell Research (IMMZ), Albert-Ludwigs-University Freiburg, Stefan-Meier-Strasse 17, 79106 Freiburg, Germany. [7]Department of Internal Medicine 5, Hematology and Oncology, Universitätsklinikum, FAU University Erlangen-Nürnberg, Ulmenweg 18, 91054 Erlangen, Germany. [8]Department of Radiology Medical Physics, University Medical Center, Freiburg, Breisacher Strasse 60a, 79106 Freiburg, Germany. [9]Institute of Pathology and Comprehensive Cancer Center, University Medical Center, Freiburg, Breisacher Strasse 115a, 79106 Freiburg, Germany. [10]Edinburgh Cancer Research Centre, Institute of Genetics & Molecular Medicine, University of Edinburgh, Crewe Road South, Edinburgh EH4 2XR, UK. [11]Department of Surgery, Universitätsklinikum, FAU University Erlangen-Nürnberg, Ulmenweg 18, 91054 Erlangen, Germany. [12]Chair of Genetics, Nikolaus-Fiebiger-Center for Molecular Medicine, Department Biology, FAU University Erlangen-Nürnberg, Glückstrasse 6, 91054 Erlangen, Germany. [13]These authors jointly supervised this work.
[14]Correspondence should be addressed to M.P.S. or T.B. (e-mail: marc.stemmler@fau.de or thomas.brabletz@fau.de)

Received 30 September 2016; accepted 16 March 2017; published online 17 April 2017; DOI: 10.1038/ncb3513

could confirm (Supplementary Fig. 1a,b). To prove the role of Zeb1 in the progression towards metastasis, we generated a conditional knockout allele of *Zeb1* (*Zeb1*^{fl}) (Fig. 1a). Cre-mediated zygotic deletion of *Zeb1* phenocopied the described developmental defects of a conventional *Zeb1* knockout[11], thereby confirming its loss of function[12]. We crossed the floxed *Zeb1* allele homozygously into KPC mice (*Pdx1-cre*;*Kras*$^{LSL.G12D/+}$;*Tp53*$^{LSL.R172H/+}$) to generate KPC;*Zeb1*$^{fl/fl}$ mice (termed KPCZ) (Fig. 1a). Progeny were born in expected ratios and showed no obvious functional defects of the pancreas. Similarly to KPC mice, all KPCZ mice developed pancreatic cancer. Notably, no significant differences from KPC were detected for a heterozygous *Zeb1* loss (KPC;*Zeb1*$^{fl/+}$) (KPCz) (Supplementary Fig. 1c); therefore, KPCz mice were merged with *Zeb1* wild-type genotypes (KPC) for all analyses. Loss of Zeb1 expression in KPCZ tumour cells was confirmed by immunohistochemistry (Supplementary Figs 1b and 2). It was associated with a reduced expression of the EMT-activators Zeb2, Slug and tentatively also Snail, but the expression frequency of Twist was maintained (Supplementary Fig. 3a). Depletion of *Zeb1* did not delay the onset and only insignificantly reduced the growth rate of primary tumours (Fig. 1b). In line with this, the number of Ki67^{+} proliferating tumour cells, as well as the spontaneous apoptotic rate and the blood vessel density, did not significantly differ (Supplementary Fig. 2). However, *Zeb1* deletion strongly influenced tumour differentiation. Whereas KPC tumours were often high grade and showed a high intra- and intertumorous heterogeneity, the number of high-grade tumours in KPCZ animals was strongly reduced and the tumours displayed homogeneous, mostly differentiated phenotypes (Fig. 1c,d and Supplementary Figs 1b and 2). Better differentiation was also associated with a significantly higher Gata6 expression (Supplementary Fig. 3b), which is a marker for higher differentiation and better clinical prognosis of human PDAC[13]. KPCZ mice showed an increased deposition of extracellular matrix (Supplementary Fig. 2). Future work will address this aspect, since the different composition of the stroma in pancreatic cancer can be associated with increased[14,15] or reduced[16,17] aggressiveness.

Next we analysed whether depletion of *Zeb1* affects malignant tumour progression. Primary KPCZ tumours showed markedly lower local invasion (Fig. 1d). Of note, differentiated KPC tumours also often underwent a dedifferentiation associated with upregulation of Zeb1 expression in invasive tumour cells. This was not detected in KPCZ tumours, a first sign for reduced plasticity in *Zeb1*-depleted cancer cells (Fig. 1e). A major finding was that the capacity for distant metastasis was strongly reduced in KPCZ tumours (Fig. 1f and Supplementary Table 1). Thereby the corresponding metastases showed a histology and Zeb1 expression state similar to that of the primary tumour (Fig. 1g and Supplementary Fig. 3c). In summary, *Zeb1* depletion strongly reduced progression towards highly malignant, metastatic pancreatic tumours. This is in stark contrast to depletion of *Snai1* or *Twist1* in the same model, which did not affect malignant tumour progression[8].

Zeb1 depletion reduces stemness, tumorigenic and colonization capacities

To further investigate the consequences of *Zeb1* depletion, we isolated primary tumour cells from KPC and KPCZ mice. In agreement with the strong heterogeneity of the KPC primary tumours, corresponding tumour cells displayed highly variable phenotypes from mesenchymal, to mixed and epithelial. This was evident from the growth patterns, as well as the expression of epithelial and mesenchymal marker genes (Fig. 2a–d and Supplementary Fig. 4a). In contrast, all tumour lines derived from KPCZ mice were fixed in an epithelial state with strongly reduced mesenchymal gene expression. However, despite the strong phenotypical differences between KPC and KPCZ-derived cancer cell lines, we detected no consistent difference in proliferation (Fig. 2e). Accordingly, the sensitivity to the chemotherapeutic agent gemcitabine, which targets proliferating cells, was variable, but not consistently changed between KPC and KPCZ cancer cells. This was also the case for two pancreatic cancer cell lines isolated from KPC tumours with depletion of *Snai1* (KPCS) (Supplementary Fig. 4b). KPCZ cells were tentatively more resistant to the epidermal growth factor receptor inhibitor erlotinib, but we did not detect a significant difference between KPC and KPCS cells. Upon subcutaneous grafting into syngeneic mice at high injection dose (1×10^5 cells), all KPC and KPCZ cell lines gave rise to tumours mimicking the differentiation state of the cell line and the growth pattern of the corresponding primary tumour, supporting the *in vitro* data on differentiation and proliferation (Supplementary Fig. 4a,c,d).

Strikingly, although all tumour cell lines showed no significant changes in proliferation and were able to grow subcutaneously, the lung colonization capacity after intravenous injection was almost completely eradicated for all KPCZ cell lines (Fig. 3a). This was not due to differences in the ability to reach the lung, since there was no significant reduction of disseminated cancer cells in the lung (Fig. 3b and Supplementary Fig. 5a). Notably, in comparison to KPCZ lines, genetic depletion of *Snai1* (KPCS cells) had no effect on lung colonization capacity (Fig. 3c), confirming data of ref. 8. This goes along with considerably high, albeit varying levels of Zeb1 expression in the KPCS lines, which might explain the maintained colonization capacity. The relevance of Zeb1 expression even at reduced levels was further demonstrated in KPC cells after partial depletion of Zeb1 to 30–50% of the original levels, which did not significantly affect the lung colonization capacity (Fig. 3d).

Since crucial traits for distant colonization include stemness and tumorigenicity, we tested these features. Tumorigenicity of the cell lines was significantly reduced in KPCZ cell lines, particularly when compared with the KPC cell lines with a similar epithelial phenotype (Supplementary Fig. 5b). Interestingly, within the KPC cell lines the epithelial differentiated cells had a higher tumorigenic capacity when compared with mesenchymal-type cell lines. This is in agreement with data showing that the plasticity of re-epithelialization is important to some degree for tumorigenic and colonization capacity and that non-plastic mesenchymal cells do not efficiently metastasize[18–20]. In addition, depletion of *Zeb1* almost completely destroyed the sphere-forming capacity, a surrogate test for stemness competence (Fig. 3e and Supplementary Fig. 5c). Analysis of established marker combinations[21] for human pancreatic cancer stem cells displayed no significant differences for CD24/CD44 and CD133. EpCAM, another marker, was not applicable, since it is a direct target of Zeb1 repression[22] and thus strongly upregulated in KPCZ cells (Supplementary Fig. 5d). This is in line with data showing that human PDAC stemness markers are not applicable in the KPC model[23]. However, the stem-cell marker Sox2 turned out to be completely

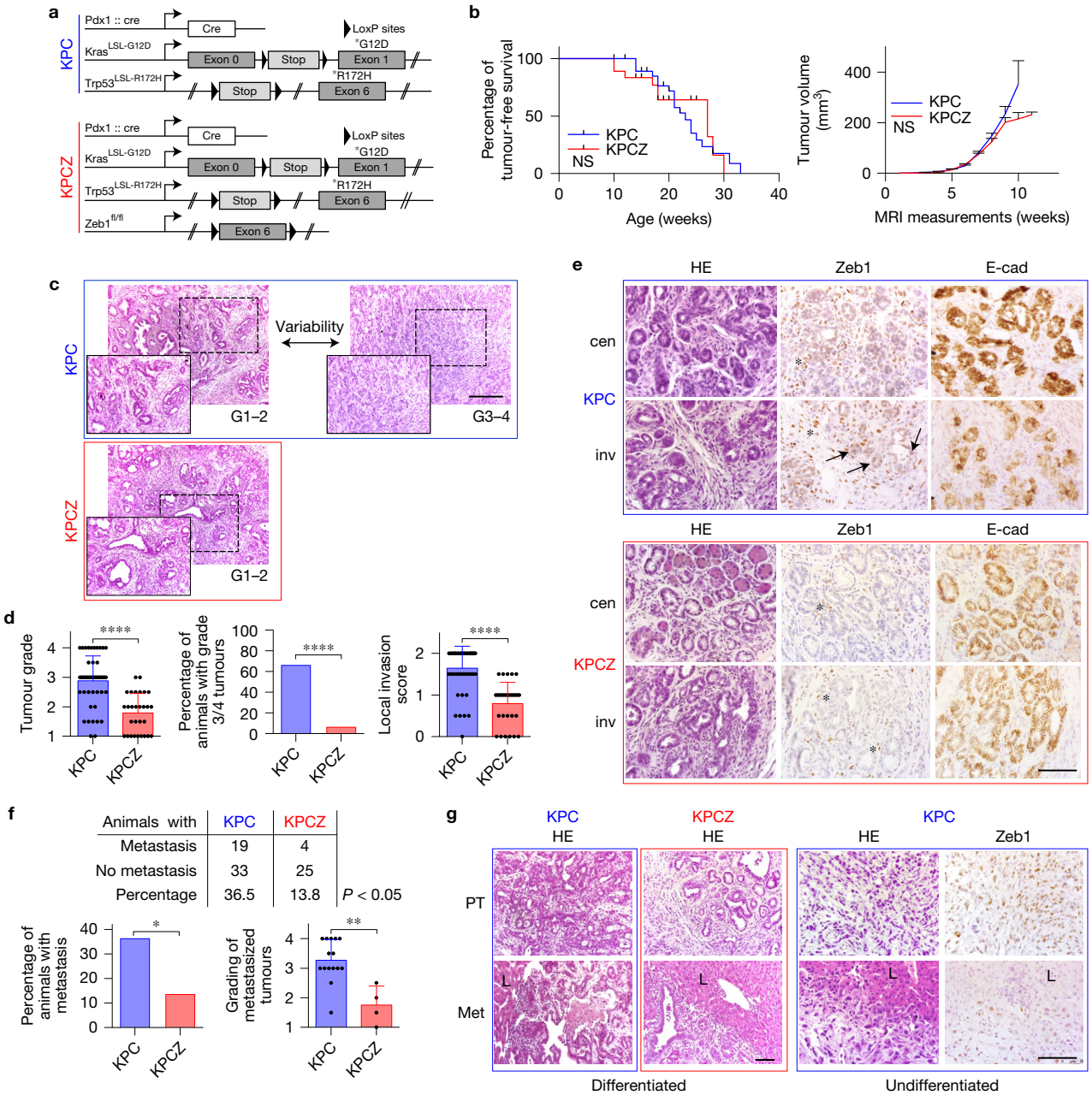

Figure 1 *Zeb1* depletion reduces invasion and metastasis in pancreatic cancer. (**a**) Scheme of the genetic mouse models for pancreatic cancer. The colour code (blue, KPC; red, KPCZ) is used for all results. (**b**) Tumour-free survival ($n = 28$ KPC, 18 KPCZ; log-rank (Mantel–Cox) test) and tumour volume (0, start of magnetic resonance imaging (MRI) measurements; $n = 23$ KPC, 27 KPCZ; error bars show mean ± s.e.m.; multiple *t*-tests with correction for multiple comparison using the Holm–Sidak method). NS, not significant. (**c**) Representative haematoxylin and eosin (HE)-stained sections for the grading of the respective tumours ($n = 48$ KPC, 29 KPCZ independent tumours). Scale bar, 250 μm and 125 μm for higher magnifications. (**d**) Grading and local invasion of the respective tumours ($n = 48$ KPC, 29 KPCZ independent tumours; error bars show mean ± s.d.; Mann–Whitney test (two tailed), chi-square test (two tailed) for grade 3/4 tumours), $^{****}P < 0.0001$. (**e**) Representative immunohistochemical stainings of consecutive sections showing nuclear Zeb1 in tumour cells (arrows) of invasive tumour regions in KPC, but not in KPCZ mice ($n = 15$ KPC, 13 KPCZ independent tumours). Asterisks mark Zeb1 expression in stromal cells, cen (central) and inv (invasive tumour regions). Scale bar, 75 μm. (**f**) Numbers and grading of metastasized tumours ($n = 52$ KPC, 29 KPCZ independent tumours; error bars, mean ± s.d.; chi-square test (two tailed) for metastasis, Mann–Whitney test (two tailed) for grading). (**g**) Representative images of differentiated (KPC and KPCZ) and undifferentiated (KPC) primary tumours (PT) and corresponding metastases (Met) with the same phenotype (L, liver) ($n = 19$ KPC, 4 KPCZ independent tumours and corresponding metastases). Scale bar, 150 μm.

absent from KPCZ cell lines and subcutaneous grafted tumours, in contrast to KPC cell lines (Fig. 3f,g). Strongly reduced Sox2 expression on *Zeb1* depletion was also reflected in the primary KPC tumours (Supplementary Fig. 2). Sox2 expression was proposed to be stabilized by Zeb1, through its reciprocal feedback loop with miR-200 family members[24]. We confirmed this hypothesis by showing that miR-200c,

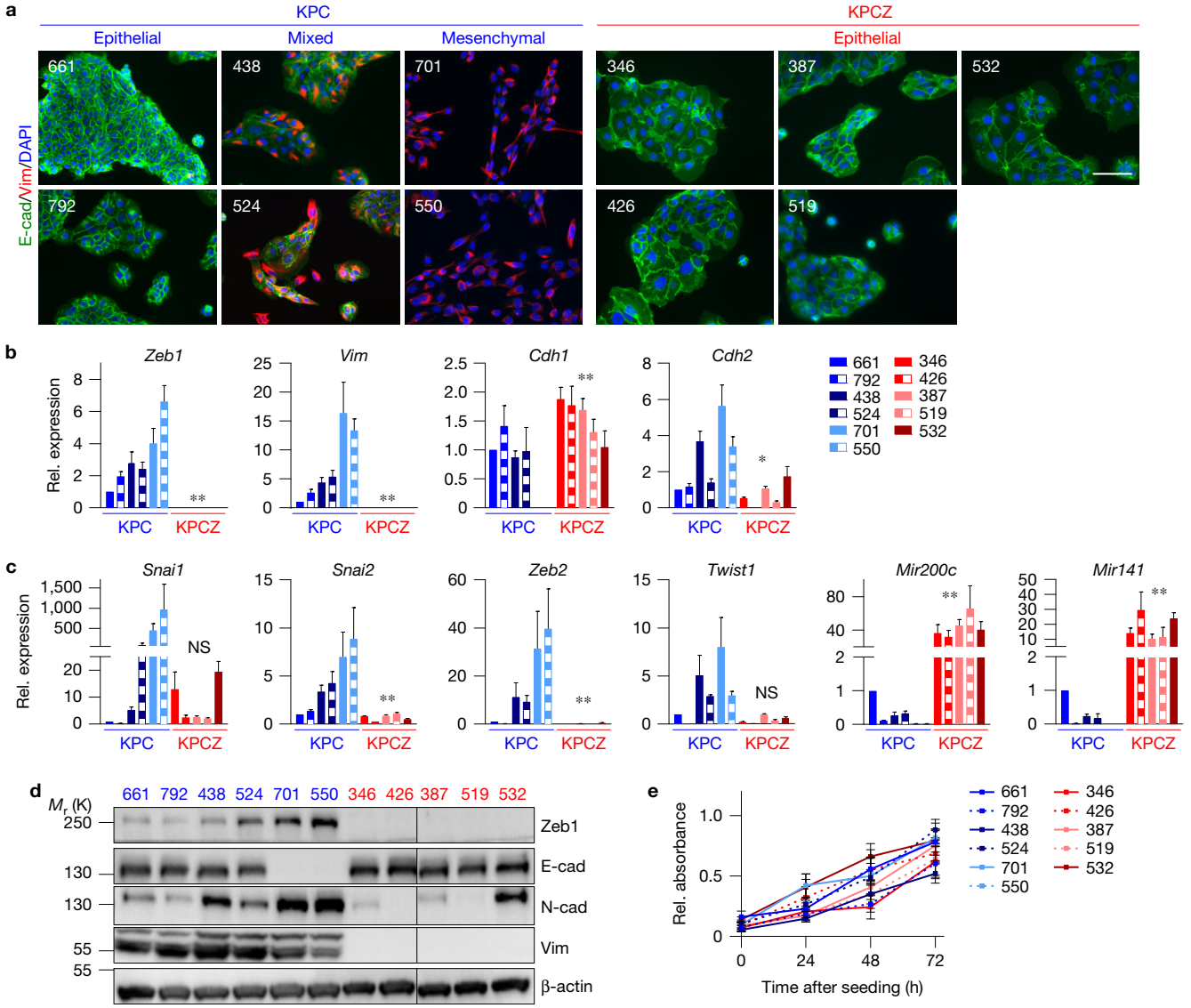

Figure 2 Depletion of *Zeb1* affects phenotypic variability of tumour cells. (**a**) Anti-E-cadherin and anti-vimentin immunofluorescence stainings showing variable expression in KPC cell lines, and homogeneous E-cadherin and lack of vimentin expression in all KPCZ cell lines. DAPI, 4,6-diamidino-2-phenylindole. Scale bar, 100 μm. (**b**) Relative messenger RNA expression levels of indicated marker genes in the isolated tumour cells. (**c**) Relative mRNA expression levels for EMT transcription factors and epithelial microRNAs. The mRNA level of cell line 661 was set to 1. $n=3$ biologically independent experiments, error bars, mean ± s.e.m. $^{*}P<0.05$, $^{**}P<0.01$, NS, not significant, Mann–Whitney test (one tailed) (**b**,**c**). (**d**) Immunoblots of indicated marker genes (unprocessed scans of immunoblots are shown in Supplementary Fig. 8). (**e**) 5-bromodeoxyuridine (BrdU) proliferation assay for the isolated tumour cell lines ($n=3$ biologically independent experiments, error bars, mean ± s.e.m.). The colour code for the isolated cell lines as depicted in **b** is valid for all corresponding results.

which is strongly upregulated in KPCZ cell lines (Fig. 2c), suppressed both *Zeb1* and *Sox2* expression in KPC cell lines (Fig. 3h). These data are of particular relevance because *Sox2* expression is enhanced in aggressive subtypes of human PDACs[25–27]. Together our data indicate that Zeb1 increases the tumorigenic capacity and is crucial for colonization of distant organs. Moreover, depletion of *Zeb1* is again in stark contrast to a depletion of *Snai1* or *Twist1*, which did not affect the tumorigenic and colonization capacity.

According to these data, we wondered why we did not see an effect on the primary tumour-free survival in KPCZ mice (Fig. 1b). It is known that mutant p53 boosts tumour progression by inducing a mutator phenotype[28,29]. In addition, it was shown that mutant p53 overcomes a growth arrest in pancreatic cancer[30]. Thus we speculated that, once a precursor lesion is formed, the progression towards a highly proliferating tumour is too fast to detect changes in the initial tumorigenic capacity. Therefore, we analysed mutant *Kras* mice without the *p53* mutant allele (Pdx1-cre;*Kras*$^{LSL.G12D/+}$, termed KC). These mice develop slowly progressing acinar–ductal metaplasia (ADM)- as well as PanIN-precursor lesions, which also express Zeb1 (ref. 10). In contrast to KPCZ, KC mice with homozygous deletion of *Zeb1* (termed KCZ) showed a strongly reduced number and grading of PanIN and ADM lesions (Fig. 4a,b and Supplementary Fig. 6a). These

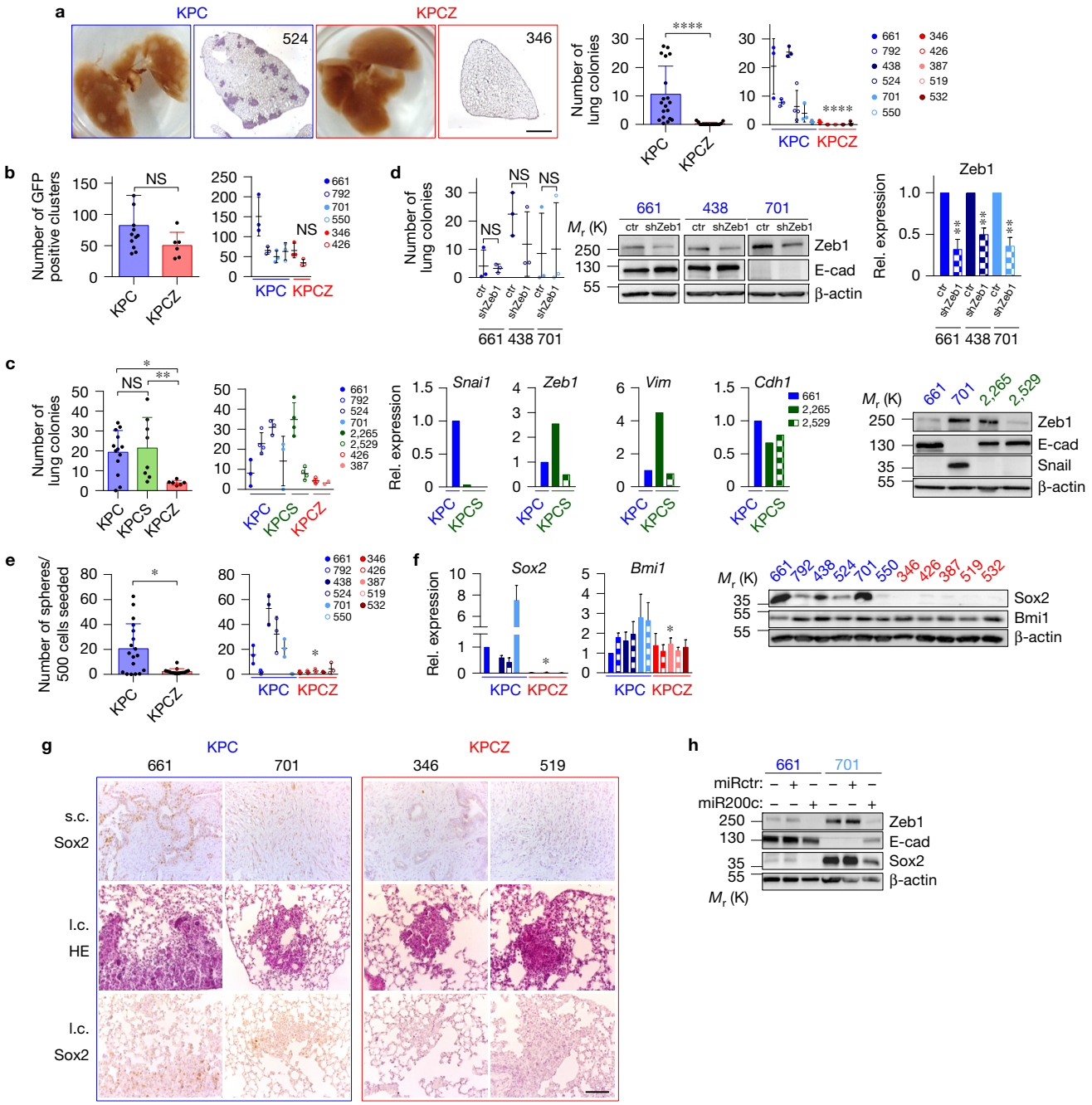

Figure 3 Depletion of *Zeb1* affects stemness, tumorigenic and colonization capacities. (**a**) Representative images of macroscopic and HE-stained lungs, 18 days after intravenous (i.v.) injection of tumour cells in syngeneic mice. Quantification of lung colonies (left, cell lines grouped by genotype; right, individual cell lines (for **a**–**c**,**e**), normalized to 20 mm^2 lung area). $n=3$ mice per cell line, $n=4$ mice for line 524, error bars, mean ± s.d.; $^{****}P<0.0001$, Mann–Whitney test (two tailed). Scale bar, 200 μm. (**b**) Number of green fluorescent protein (GFP)+ cells per visual field 2 h after i.v. injection ($n=3$ mice per cell line, error bars, mean ± s.d. Mann–Whitney test (two tailed)). (**c**) Quantification after i.v. injection of KPC, KPCS and KPCZ tumour cells in nude mice ($n=13$ mice for KPC, $n=8$ for KPCS, $n=6$ for KPCZ—four mice per cell line, Mann–Whitney test (two tailed), $^{**}P<0.01$, NS, not significant). Relative mRNA expression levels in KPCS cell lines; mRNA levels of KPC661 (expressing low levels of Snail) set to 1 (average of $n=2$ biologically independent experiments, error bars, mean ± s.d.). Immunoblot for the indicated proteins with KPC701 as control expressing high Snail levels. (**d**) Number of lung colonies after i.v. injection of KPC shcontrol (ctr) and KPC shZeb1 tumour cells in nude mice (normalized to 20 mm^2 lung area) ($n=3$ mice per cell line, error bars mean ± s.d.; Mann–Whitney test (two tailed), NS, not significant). Immunoblots and corresponding quantifications, showing short hairpin RNA (shRNA)-mediated partial reduction of Zeb1 ($n=3$ biologically independent experiments, error bars, mean ± s.e.m.; unpaired Student's *t*-test (two tailed), $^{**}P<0.01$). (**e**) Quantification of sphere-forming capacity ($n=3$ biologically independent experiments, error bars, mean ± s.d.; $^{*}P<0.05$, Mann–Whitney test (two tailed)). (**f**) Relative mRNA expression levels and immunoblots of stem-cell genes ($n=3$ biologically independent experiments, error bars, mean ± s.e.m.; $^{*}P<0.05$, Mann–Whitney test (one-tailed)). mRNA levels of line 661 set to 1. (**g**) HE and immunohistochemical staining for Sox2 in tumours grown subcutaneously ($n=51$) or in the lung ($n=36$) after i.v. injection (l.c.) of indicated cell lines. Scale bar, 100 μm. (**h**) Immunoblot for indicated proteins on overexpression of *Mir200c*. For source data for **c**,**d**,**f** see Supplementary Table 5; unprocessed scans of immunoblots are shown in Supplementary Fig. 8.

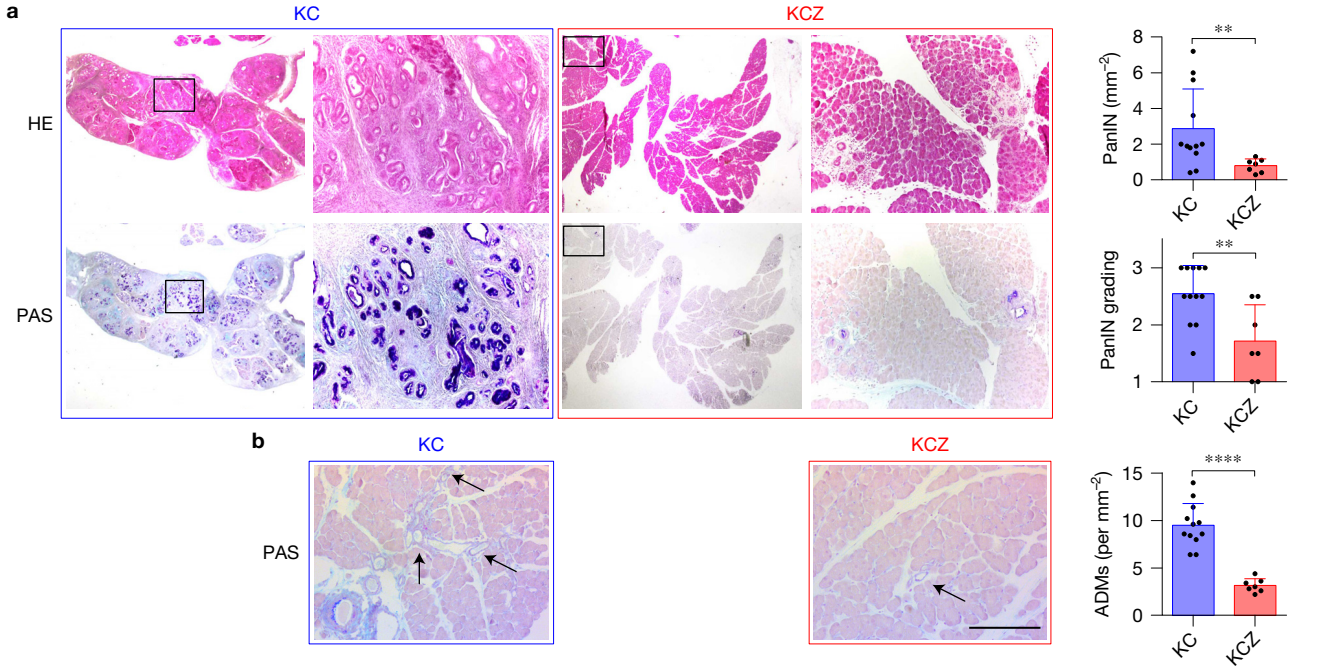

Figure 4 Depletion of *Zeb1* reduces ADM- and PanIN-precursor lesions. (**a**,**b**) Consecutive sections of representative HE- and periodic acid/Schiff's (PAS)-stained sections showing precancerous PanIN (**a**) and ADM lesions (**b**) in the pancreas of 6-month-old KC and KCZ mice. Specific dark blue/purple PAS staining indicates the mucin-rich PanIN lesions; arrows indicate ADMs. Squares mark the magnified regions; scale bars, 1 mm and 150 μm for higher magnifications in **a** and 75 μm in **b**. Quantification of the ADM and PanIN areas and PanIN grading is given. $n = 12$ KC and 7 KCZ independent mice, error bars, mean ± s.d.; $^{**}P < 0.01$, $^{****}P < 0.0001$; unpaired Student's *t*-test (two tailed) with Welch's correction for ADM and PanIN areas and Mann–Whitney test (two tailed) for grading.

data further indicate that Zeb1 triggers the tumorigenic capacity in pancreatic cancer from initial development until late-stage metastasis.

Zeb1 is crucial for cancer cell plasticity

Zeb1 affects expression not of single genes or small gene clusters but of thousands of genes, leading to a complete reprogramming of cells[31], and we have shown that Zeb1 exerts pleiotropic effects on many different programs and pathways[31–33]. Therefore, we carried out a global gene-expression analysis to examine the impact of Zeb1 on cell plasticity. A principal-component analysis (PCA) showed a clear separation of KPC and KPCZ cell lines and a separation of the epithelial and mesenchymal phenotype along the first (PC1) and second principal components (PC2), respectively (Fig. 5a). The latter verified the initial findings that a depletion of *Zeb1* fixes the cells in a homogeneous epithelial state, indicating that Zeb1 is a critical factor underlying cell heterogeneity and potentially also plasticity. In line with the PCA, a gene-set enrichment analysis (GSEA) confirmed that *Zeb1* depletion shifts the cells towards an epithelial phenotype (Supplementary Fig. 6b). Moreover, loss of *Zeb1* expression enriches for genes associated with addiction to *Kras* expression[34], and reduced metastatic competence[35], as well as the 'classical' subtype of human PDACs, which has the best clinical prognosis[36] (Fig. 5b). We further analysed the expression of genes strongly associated with metastatic progression, including *Pdgfrb*, which is essential to drive metastasis in pancreatic cancer together with mutant p53 (ref. 37). All of the analysed genes were expressed in KPC cell lines, but strongly downregulated on *Zeb1* depletion (Fig. 5c). However, in agreement with the heterogeneous phenotypes, these pro-metastatic genes were expressed only at low levels in KPC tumour cells with epithelial differentiation, although these cell lines had the highest lung-colonization capacity. We hypothesized that epithelial KPC cells possess enough plasticity to adapt their gene expression.

Enhanced plasticity of cancer cells is considered an important driving force of malignant tumour progression, allowing continuous adaptions to the demanding conditions in the changing tumour environment[1,38,39]. We have previously demonstrated that ZEB1, particularly through its feedback loop with miR-200 family members, is a motor of cellular plasticity in response to extracellular cues[4]. Thus, we assumed that the presence of Zeb1 allows adaptations of gene-expression patterns and that loss of cellular plasticity is an important consequence of *Zeb1* depletion in cancer cells. We tested this hypothesis by treating KPCZ cells with TGFβ1, a driver of malignant tumour progression and prominent inducers of EMT (refs 40,41). As expected, on TGFβ treatment KPC cells with an epithelial phenotype underwent an EMT. However, even after long-term TGFβ treatment, KPCZ cells maintained their epithelial phenotype (Fig. 6a,b and Supplementary Fig. 7a). Thus, without Zeb1, the cells were locked in their phenotypic state and lost plasticity. Loss of plasticity was also reflected in TGFβ-induced changes in global gene expression, where, in contrast to KPC cell lines with an epithelial phenotype, the epithelial KPCZ cell lines displayed a strongly reduced responsiveness to TGFβ (Fig. 6c). The PCA showed an induction of a mesenchymal phenotype only of the KPC cell lines under TGFβ stimulation along the first principal component (PC1). Among the 20,052 analysed genes, 1,514

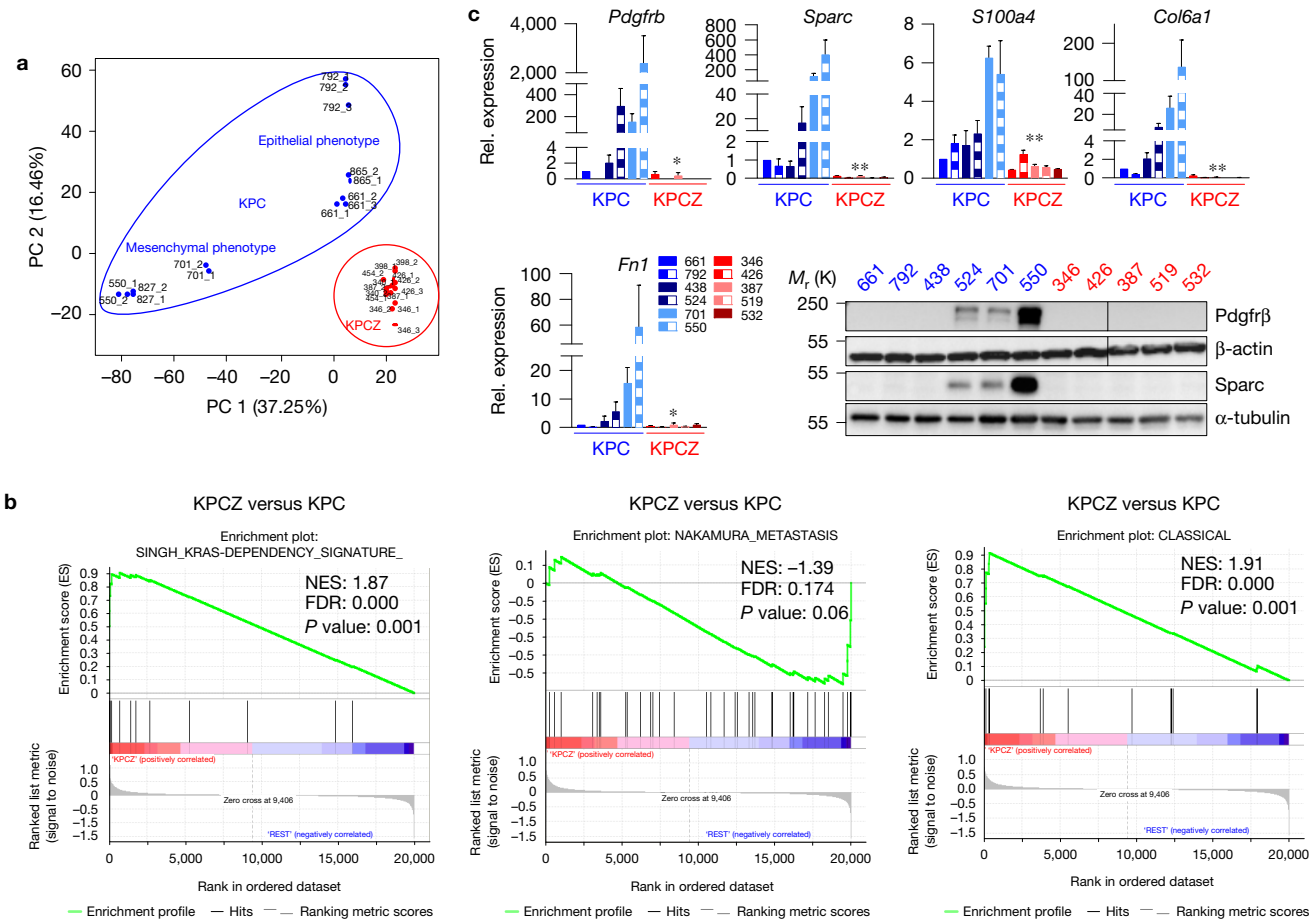

Figure 5 Depletion of *Zeb1* reduces phenotypic variability. (**a**) PCA of the KPC and KPCZ cell-line transcriptomes. The plot depicts the first two principal components using all samples, accounting for about 44% and about ∼17% of the variance, respectively. (**b**) GSEAs of transcriptome data from KPCZ versus KPC cells reveal enrichment of gene signatures associated with Kras dependency and the classical type of pancreatic cancer, as well as a reduction of genes associated with metastasis in KPCZ cell lines. NES, normalized enrichment score; FDR, false-discovery rate. (**c**) Relative mRNA expression levels (quantitative PCR with reverse transcription, qRT–PCR) and immunoblots of indicated genes associated with metastasis in the isolated tumour cells ($n=3$ biologically independent experiments, error bars, mean ± s.e.m.; $^{*}P<0.05$, $^{**}P<0.01$, Mann–Whitney test (one-tailed)). The mRNA level of cell line 661 was set to 1. Unprocessed scans of immunoblots are shown in Supplementary Fig. 8.

were significantly regulated on long-term TGFβ treatment (Fig. 6c and Supplementary Table 2); however, 1,377 (91%) of them depended on the genetic presence of *Zeb1*. The genes associated with metastatic progression, including *Pdgfrb*, which were not present in epithelial KPC cells, were also upregulated by TGFβ in a Zeb1-dependent manner (Fig. 6d). These data also indicate that Zeb1 is important for a large fraction of TGFβ-induced changes. The Zeb1-dependent TGFβ-induced genes also included genes that we recently identified as common Zeb1/Yap target genes upregulated in aggressive cancer types (Supplementary Fig. 7b)[31]. The high Zeb1-dependent plasticity was further indicated by the fact that Zeb1-associated phenotypic and gene-expression changes were reversible after withdrawal of TGFβ (Fig. 6e–g).

Another important aspect of cancer cell biology is metabolics. Tumour cells show a high metabolic plasticity in reacting to environmental changes on their way to metastasis[42]. We exemplified this by modulating the two basic energy consumption pathways: glycolysis and oxidative phosphorylation (OXPHOS). As measured in a mitochondrial stress test, KPCZ cells have a lower basal respiration and respiration-related ATP production as indication of reduced OXPHOS (Fig. 7a), which is also visible in a glycolysis stress test (Fig. 7b). Blocking of OXPHOS by oligomycin in a glycolysis stress test forces cells to exploit their glycolytic capacity for fulfilling energy demands and demonstrates a considerable glycolytic reserve in KPC cells (Fig. 7b). However, this glycolytic switch was no longer possible in KPCZ cells, owing to a complete lack of a glycolytic reserve. Thus, the plasticity in switching between basic energy pathways and adapting to different oxygen availability was also strongly dependent on the expression of *Zeb1*.

Finally, high phenotypic plasticity of epithelial KPC cells was also detected *in vivo* after grafting into syngeneic mice. Although they displayed a differentiated phenotype in central tumour regions, KPC tumour cells underwent a dedifferentiation associated with an upregulation of Zeb1 at the invasive front. In contrast, grafted KPCZ cell lines displayed no phenotypic plasticity, but were fixed in their differentiated state (Fig. 7c and Supplementary Fig. 7c). Altogether, the data indicate that Zeb1 is very important for cellular plasticity in pancreatic cancer cells.

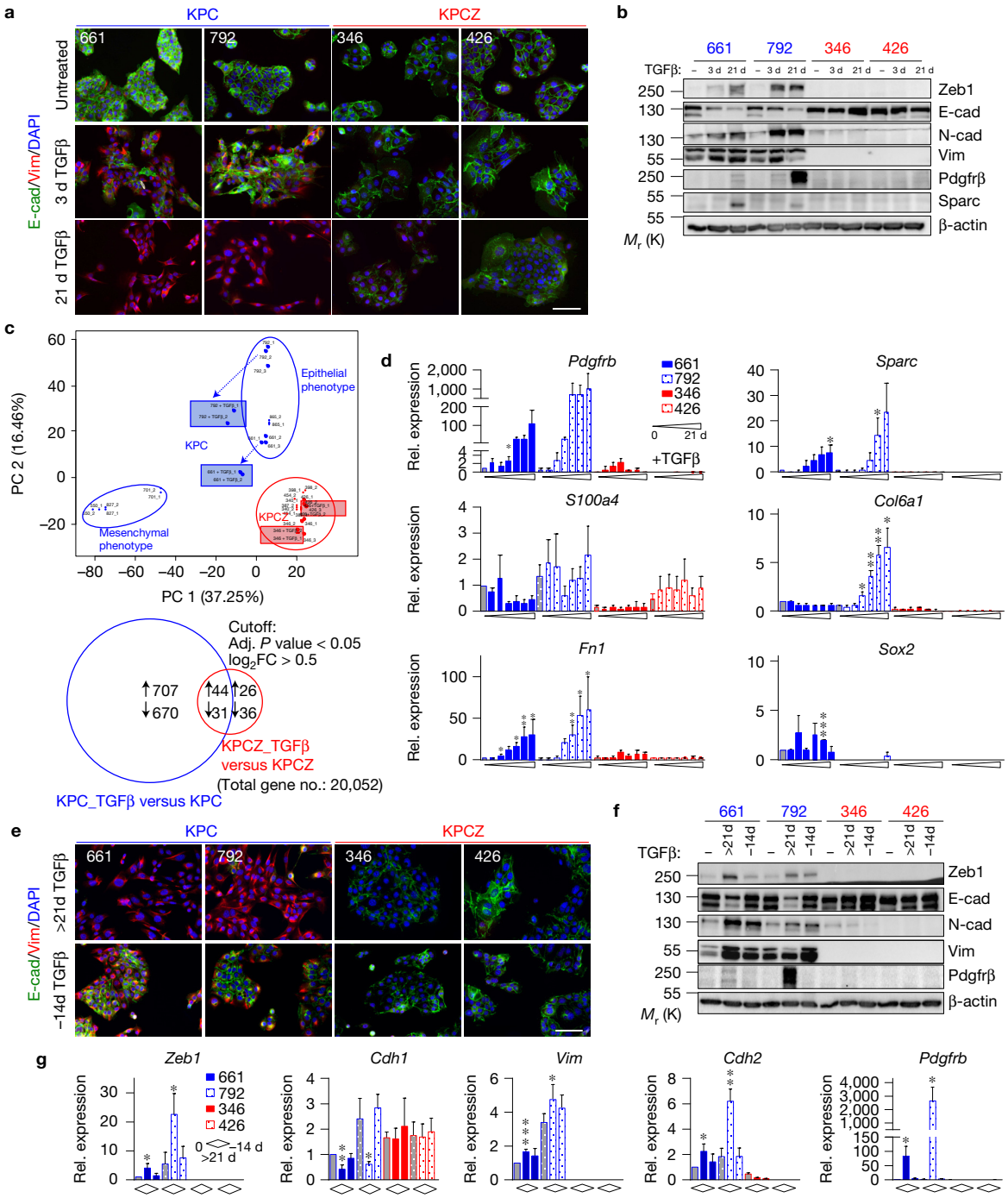

Figure 6 Depletion of *Zeb1* reduces TGFβ-induced cellular plasticity. (**a**) Anti-E-cadherin and anti-vimentin immunofluorescence staining of two epithelial KPC and two KPCZ cancer cell lines treated with TGFβ1 for 3 and 21 days. Scale bar, 100 μm. (**b**) Immunoblots for indicated marker genes of the same lines as in **a**. Unprocessed scans of immunoblots are shown in Supplementary Fig. 8. (**c**) PCA of transcriptome signatures of the KPC and KPCZ cell lines on TGFβ treatment. TGFβ-induced shifts in expression of the cell lines shown in **a** are marked with coloured boxes (microarrays carried out in duplicate, referred to as TGFβ_1 and TGFβ_2). Note a great shift towards a mesenchymal pattern for KPC cell lines but not for KPCZ lines (upper panel). Venn diagram showing a number of genes significantly up- or downregulated (cutoff: adjusted $P < 0.05$ and $\log_2 FC > 0.5$) by 14 days of TGFβ treatment of cell lines shown in **a**. Moderated *t*-test (lower panel). (**d**) Relative mRNA expression levels (qRT–PCR) of indicated genes (including the metastasis set in Fig. 5c) in KPC and KPCZ cell lines treated for different times with TGFβ (times: 0, 6 h, 1, 3, 7, 14, 21 days) ($n = 3$ biologically independent experiments, error bars, mean ± s.e.m.). mRNA levels of cell line 661 at day 0 were set to 1. Statistical analysis is shown for the comparison of TGFβ treated and untreated samples (grey bars) of each individual cell line. $^{*}P < 0.05$, $^{**}P < 0.01$, unpaired Student's *t*-test (one-tailed). (**e**) Anti-E-cadherin and anti-vimentin immunofluorescence staining of two epithelial KPC and two KPCZ cancer cell lines treated with TGFβ for more than 21 days (>21 d) followed by 14 days TGFβ withdrawal (−14 d). Scale bar, 100 μm. (**f**,**g**) Immunoblots (**f**) and relative mRNA expression levels (qRT–PCR) (**g**) of indicated marker genes of the same cell lines as in **e** ($n = 3$ biologically independent experiments, error bars, mean ± s.e.m.; $^{*}P < 0.05$, $^{**}P < 0.01$, $^{***}P < 0.001$, unpaired Student's *t*-test (one-tailed)). mRNA levels of cell line 661 at day 0 were set to 1. For source data for Fig. 5d,f see Supplementary Table 5; unprocessed scans of immunoblots are shown in Supplementary Fig. 8.

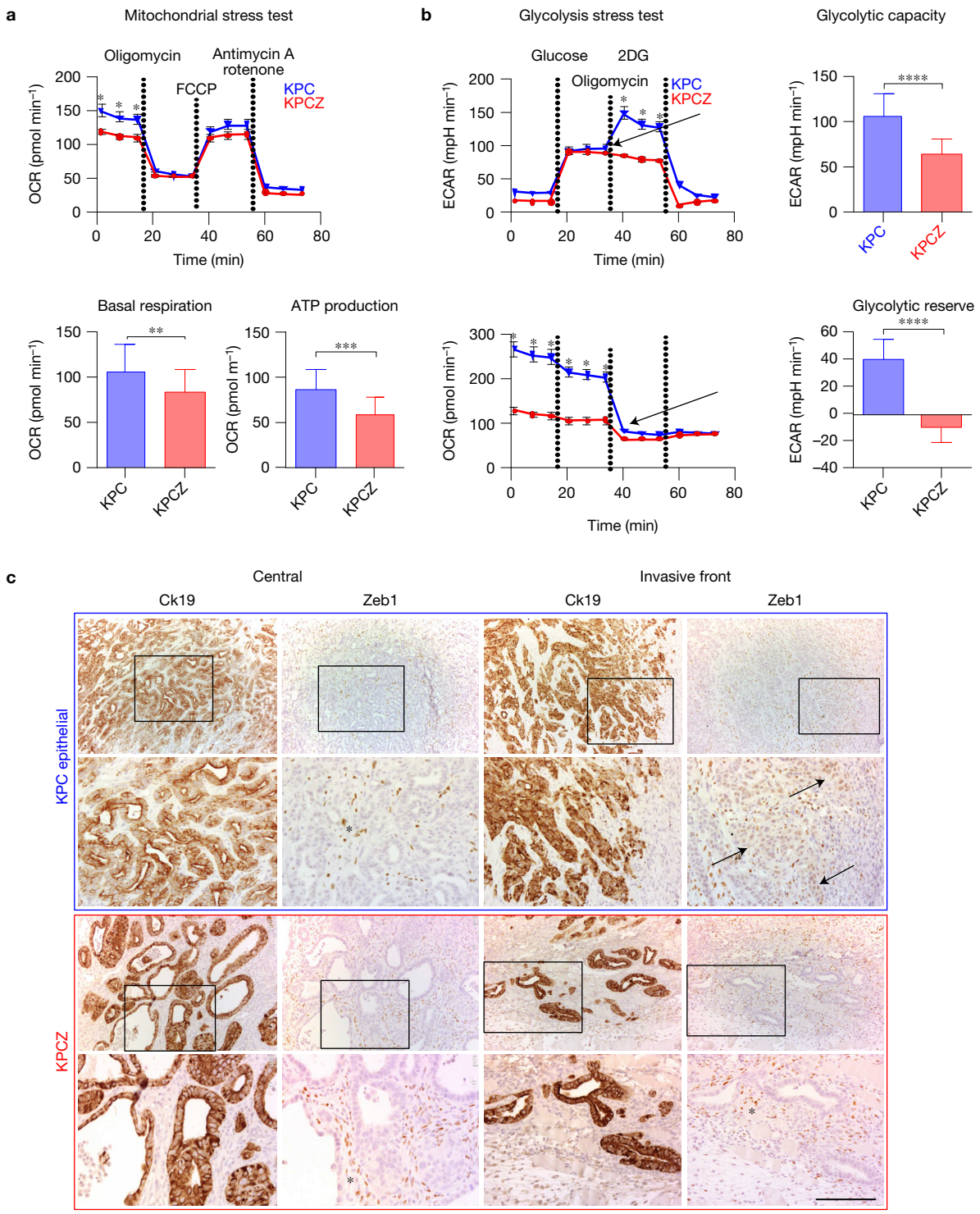

Figure 7 Depletion of *Zeb1* reduces metabolic and phenotypic plasticity. (**a**) Mitochondrial stress test (MST) showing the oxygen consumption rate (OCR) as an indicator for OXPHOS and deduced levels for basal respiration and ATP production. (**b**) Glycolysis stress test (GST) showing the extracellular acidification rate (ECAR) as an indicator for glycolysis and the OCR after glucose stimulation, blocking of oxidative phosphorylation with oligomycin and blocking of glycolysis with 2-deoxy-glucose (2DG), as well as deduced glycolytic capacity and glycolytic reserve ($n=7$ biologically independent experiments; error bars, ± s.e.m. for MST and GST and ± s.d. for other parameters; for MST and GST a multiple *t*-test with correction for multiple comparison using the Holm–Sidak method was used; for other parameters an unpaired Student's *t*-test (two tailed) was used; $^{*}P<0.05$, $^{**}P<0.01$, $^{***}P<0.001$, $^{****}P<0.0001$). Note a complete lack of a glycolytic reserve (upper arrow) after blocking oxidative phosphorylation (lower arrow) in KPCZ cells. KPC661 and 792 as well as all KPCZ cell lines were used. (**c**) Representative images of consecutive sections of immunohistochemical stainings for Ck19 and Zeb1, comparing the plasticity of Zeb1 expression in central and invasive tumour regions. Shown are tumours derived from one KPC and one KPCZ cell line. Asterisks label Zeb1 expression in stromal cells; arrows indicate Zeb1-positive tumour cells at the invasive front. Ck19 expression is shown to identify cancer cells. $n=15$ KPC, 13 KPCZ independent tumours, Scale bars, 50 μm and 150 μm for higher magnifications.

Table 1 Summary of the differential behaviour of KPC versus KPCZ cell lines concerning crucial traits for tumour progression towards metastasis.

Genotype	Phenotype	Cell line	Sphere formation	Tumorigenicity	Plasticity	Lung colonization	Lung dissemination
KPC	Epithelial	661	++	+++	+++	+++	+++
		792	+	+++	+++	+	++
	Mesenchymal	701	++	++	na	+	++
		550	–	+	na	–	++
KPCZ	Epithelial	346	–	+	–	–	++
		426	–	+	–	–	++

For experimental data on sphere formation see Fig. 3e and Supplementary Fig. 5c; for tumorigenicity see Supplementary Fig. 5b; for plasticity see Figs 6 and 7 and Supplementary Fig. 7a,c; for lung colonization see Fig. 3a; for lung dissemination see Fig. 3b and Supplementary Fig. 5a. (–, no capacity; +, weak capacity; ++, moderate capacity; +++, strong capacity; na, not analysed).

DISCUSSION

Here, we describe a key role for the EMT-TF Zeb1 in the *in vivo* progression of pancreatic cancer from early precursor lesions towards metastasis. Genetic depletion of *Zeb1* in the pancreas reduces formation of ADM- and PanIN-precursor lesions, undifferentiated (high-grade) carcinomas, invasion and metastasis. In isolated primary cancer cell lines *Zeb1* ablation leads to loss of cellular plasticity and fixation in an epithelial phenotype, a likely cause of reduced stemness, tumorigenicity and colonization capacities (Table 1).

Our data demonstrate that Zeb1 acts in strong contrast to the EMT-TFs Snail and Twist in pancreatic cancer. *Snai1* or *Twist1* depletion in the same KPC model did not affect formation of PanINs, tumour differentiation, invasion, colonization or importantly metastasis[8]. Based on their results, the authors of ref. 8 claimed that EMT is dispensable for metastasis. However, our data favour a different interpretation and allow a more comprehensive picture of the effect of EMT-TFs in tumours. Our results point to functional differences of EMT-TFs and demonstrate that Zeb1 stimulates pancreatic tumour progression from formation of precursor lesions to late-stage metastasis.

What could be the critical functions of Zeb1? Its regulatory potential is not limited to effects on a few crucial downstream target genes, but rather leads to a global reprogramming of gene expression patterns[31], and controls not only EMT but also other programs and pathways. One of the most striking consequences of *Zeb1* depletion was the almost complete inhibition of lung colonization. We postulate two major effects of *Zeb1* inactivation as the underlying molecular mechanism: the block in cellular plasticity, considered a major driving force of tumour progression towards metastasis and the reduction of stemness, a crucial property underlying tumorigenicity and colonization. Enhanced plasticity of cancer cells impresses as ongoing transitions between an undifferentiated/(partial) mesenchymal and a differentiated/epithelial phenotype[1,38,39,43,44]. We here describe a central role of Zeb1 in exerting different aspects of cellular plasticity, particularly the response to TGFβ, but also to metabolic changes and changes in the *in vivo* intratumorous heterogeneity. Differentiated KPC as well as KPCZ cancer cells expressed only low levels of metastasis-associated genes. However, only KPC cells, and not KPCZ cells, were able to activate their expression on TGFβ treatment. These genes include *Pdgfrb*, which was recently shown to be absolutely required for metastasis in *p53*-mutant pancreatic cancer[37]. As a side effect, our finding that the absence of *Zeb1* strongly reduces the number of TGFβ-regulated genes indicates that Zeb1 is important for a large part of the TGFβ response (Supplementary Table 2). Furthermore, Zeb1-linked plasticity is exemplified by its impact on central metabolic pathways. The plasticity in switching between basic energy pathways is strongly compromised in *Zeb1*-depleted cells, displaying both a reduced OXPHOS and reduced glycolytic reserve, which might also be critical for the colonization step. In addition *Zeb1* inactivation affects stemness and tumorigenic properties, supporting the view that EMT-MET dynamics also reflects the plasticity between stemness and a differentiated state[45,46]. In particular, the strong reduction of the stem cell factor Sox2 in KPCZ tumours and derived cell lines is of high relevance, since its expression was correlated with stemness, plasticity and progression in pancreatic and other cancer types[25–27]. Together, our data indicate that Zeb1 is crucial for cellular plasticity and stemness/tumorigenic properties in pancreatic cancer cells.

There are several potential reasons why Zeb1 in particular is associated with cellular plasticity. First, Zeb1 is linked in a reciprocal double-negative feedback loop with members of the miR-200 family, which controls a switch between an undifferentiated/stemness and a differentiated phenotype[4]. Second, the *Zeb1* gene itself has a poised, bivalent chromatin configuration, allowing a rapid switch between high expression in cancer stem cells and low expression in non-cancer stem cells[47]. Moreover, we are beginning to understand functional differences between Zeb1 and other EMT-TFs at the biochemical level. For instance, we have described a direct interaction of ZEB1 with the Hippo-pathway effector YAP1, which is crucial for activating a common ZEB1/YAP1 target gene set important for tumour progression[31]. Genes of this target set can be activated by TGFβ in epithelial KPC cells, but not in KPCZ cells. Notably, as demonstrated here for Zeb1, Yap1 was also shown to be important for the progression through ADM towards pancreatic carcinoma[48,49].

Zeb1-dependent gene expression signatures also point to a clinical relevance of our findings. *Zeb1* ablation is associated with tumours of the 'classical subtype' of pancreatic cancer, which has the best clinical prognosis, compared with other subtypes[36,50]. These data fit to the reduced aggressiveness of KPCZ tumours and further support data showing that *Zeb1* expression correlates with more aggressive precursor lesions and poor outcome in human pancreatic cancer[24,51,52]. Moreover, KPCZ cells show enrichment of a gene signature associated with KRAS addiction. Notably, in this study absence of ZEB1 was already a determinant of KRAS dependency[34,53]. Thus, although KRAS bears the key mutation in pancreatic cancer[54], expression of ZEB1 might render cancer cells independent of mutant KRAS.

However, our findings also raise additional questions. The first of these is why we did not observe a significant effect of *Zeb1* depletion on primary tumour-free survival in KPCZ mice (Fig. 1b). When we omitted the mutant *p53* allele, *Zeb1* was critical for the formation of Kras-driven ADM and PanIN lesions, as its depletion strongly reduced

their occurrence. Similar data were recently shown in the MMTV-PyMT model of breast cancer, where Snail was important for tumour initiation and progression in a p53 wild-type but not p53 mutant context[55]. Thus our data support the hypothesis that in the context of mutant p53 the progression towards a highly proliferating tumour is too fast to allow detection of changes in initial tumorigenicity. The second question is why we detected metastases in KPCZ animals at all. The fact that *Zeb1* loss reduces the metastatic competence to approximately 30% shows that Zeb1-associated EMT and plasticity strongly support metastasis. Nevertheless, it also indicates a Zeb1-independent, albeit less efficient, metastasis formation, which might include a potential partial redundancy with remaining EMT-TFs, although at a significantly lower efficacy. Another explanation could be different routes to metastasis, which probably cooperate with EMT-TF-dependent mechanisms to various extents. As already postulated, different routes may emerge by acquisition of additional genetic alterations driving metastasis independent of cellular-plasticity-associated traits[1,56]. Again, mutated p53 might enhance the generation of such a genetically driven metastasis[30]. In this light, the fact that *Zeb1* depletion efficiently reduces plasticity, colonization and metastasis even in the context of mutant p53 is remarkable and further supports the importance of Zeb1 as a crucial driver of tumour progression.

In conclusion, we have demonstrated that the EMT-TF Zeb1 is a key driver of pancreatic tumour progression from early tumorigenesis to late-stage metastasis, underscoring the important role of EMT activation in these processes. By contrast, Snail and Twist were shown to be dispensable for metastasis in this cancer type, indicating that EMT-TFs have specific subfunctions, which are not redundant but complementary. Non-redundant subfunctions of EMT-TFs have already been described, for example, for Zeb1 and Zeb2 in melanoma[57,58], for Snail and Slug in breast cancer[59], and for Sox4 (ref. 60) and Prrx1 (ref. 19). Moreover, subfunctions can be tissue specific, as demonstrated by the different roles of Snail in metastasis of breast[61] and pancreatic cancer[8]. Consequently, therapeutic strategies directed at EMT-TFs should consider these specificities and target such factors simultaneously. □

METHODS

Methods, including statements of data availability and any associated accession codes and references, are available in the online version of this paper.

Note: Supplementary Information is available in the online version of the paper

ACKNOWLEDGEMENTS

We thank B. Schlund, E. Bauer and J. Pfannstiel, as well as U. Appelt and M. Mroz (Core Unit Cell Sorting and Immunomonitoring, FAU Erlangen, Germany) for technical assistance and R. Eccles for critical reading of the manuscript. We are grateful to D. Saur (Department of Internal Medicine, TU Munich, Germany) for providing the KPCS cell lines. We thank J. C. Wu, from Stanford University, for the MSCV-LUC_EF1-GFP-T2A-Puro plasmid. This work was supported by grants to T.B., S.B., M.B. and M.P.S. from the German Research Foundation (SFB850/A4, B2, Z1 and DFG BR 1399/9-1, DFG 1399/10-1, DFG BR4145/1-1) and from the German Consortium for Translational Cancer Research (DKTK).

AUTHOR CONTRIBUTIONS

A.M.K. planned and carried out experiments and wrote the manuscript. J.M. carried out mouse experiments. M.L.L. carried out drug studies. O.S. generated the floxed Zeb1 allele. M.B. and H.B. carried out bioinformatics analyses. M.B. and D.M. carried out metabolic tests. W.R. carried out MRI analyses. P.B. carried out histological analyses. V.G.B. established mouse models. C.P. generated cell lines. T.H.W. carried out mouse experiments. S.B. generated the floxed Zeb1 allele, and planned and carried out experiments. M.P.S. generated the floxed Zeb1 allele, planned and carried out mouse experiments, was involved in coordination and wrote the manuscript. T.B. planned and coordinated the project, analysed data and wrote the manuscript. M.P.S. and T.B. contributed equally and share senior authorship.

COMPETING FINANCIAL INTERESTS

The authors declare no competing financial interests.

Published online at http://dx.doi.org/10.1038/ncb3513
Reprints and permissions information is available online at www.nature.com/reprints

1. Brabletz, T. To differentiate or not—routes towards metastasis. *Nat. Rev. Cancer* **12,** 425–436 (2012).
2. Kalluri, R. & Weinberg, R. A. The basics of epithelial-mesenchymal transition. *J. Clin. Invest.* **119,** 1420–1428 (2009).
3. Nieto, M. A., Huang, R. Y.-J., Jackson, R. A. & Thiery, J. P. EMT: 2016. *Cell* **166,** 21–45 (2016).
4. Brabletz, S. & Brabletz, T. The ZEB/miR-200 feedback loop–a motor of cellular plasticity in development and cancer? *EMBO Rep.* **11,** 670–677 (2010).
5. Vandewalle, C., Van Roy, F. & Berx, G. The role of the ZEB family of transcription factors in development and disease. *Cell. Mol. Life Sci.* **66,** 773–787 (2009).
6. Zhang, P., Sun, Y. & Ma, L. ZEB1: at the crossroads of epithelial-mesenchymal transition, metastasis and therapy resistance. *Cell Cycle* **14,** 481–487 (2015).
7. Fischer, K. R. *et al.* Epithelial-to-mesenchymal transition is not required for lung metastasis but contributes to chemoresistance. *Nature* **527,** 472–476 (2015).
8. Zheng, X. *et al.* Epithelial-to-mesenchymal transition is dispensable for metastasis but induces chemoresistance in pancreatic cancer. *Nature* **527,** 525–530 (2015).
9. Hingorani, S. R. *et al.* Trp53R172H and KrasG12D cooperate to promote chromosomal instability and widely metastatic pancreatic ductal adenocarcinoma in mice. *Cancer Cell* **7,** 469–483 (2005).
10. Rhim, A. D. *et al.* EMT and dissemination precede pancreatic tumor formation. *Cell* **148,** 349–361 (2012).
11. Higashi, Y. *et al.* Impairment of T Cell Development in deltaEF1 Mutant Mice. *J. Exp. Med.* **185,** 1467–1480 (1997).
12. Brabletz, S. *et al.* Generation and characterization of mice for conditional inactivation of Zeb1. *Genesis* http://dx.doi.org/10.1002/dvg.23024 (2017).
13. Martinelli, P. *et al.* GATA6 regulates EMT and tumour dissemination, and is a marker of response to adjuvant chemotherapy in pancreatic cancer. *Gut* http://dx.doi.org/10.1136/gutjnl-2015-311256 (2016).
14. Laklai, H. *et al.* Genotype tunes pancreatic ductal adenocarcinoma tissue tension to induce matricellular fibrosis and tumor progression. *Nat. Med.* **22,** 497–505 (2016).
15. Erkan, M. *et al.* The activated stroma index is a novel and independent prognostic marker in pancreatic ductal adenocarcinoma. *Clin. Gastroenterol. Hepatol.* **6,** 1155–1161 (2008).
16. Özdemir, B. C. *et al.* Depletion of carcinoma-associated fibroblasts and fibrosis induces immunosuppression and accelerates pancreas cancer with reduced survival. *Cancer Cell* **25,** 719–734 (2014).
17. Rhim, A. D. *et al.* Stromal elements act to restrain, rather than support, pancreatic ductal adenocarcinoma. *Cancer Cell* **25,** 735–747 (2014).
18. Tsai, J. H., Donaher, J. L., Murphy, D. A., Chau, S. & Yang, J. Spatiotemporal regulation of epithelial-mesenchymal transition is essential for squamous cell carcinoma metastasis. *Cancer Cell* **22,** 725–736 (2012).
19. Ocaña, O. H. *et al.* Metastatic colonization requires the repression of the epithelial-mesenchymal transition inducer Prrx1. *Cancer Cell* **22,** 709–724 (2012).
20. Korpal, M. *et al.* Direct targeting of Sec23a by miR-200s influences cancer cell secretome and promotes metastatic colonization. *Nat. Med.* **17,** 1101–1108 (2011).
21. Raj, D., Aicher, A. & Heeschen, C. Concise review: stem cells in pancreatic cancer: from concept to translation. *Stem Cells* **33,** 2893–2902 (2015).
22. Vannier, C., Mock, K., Brabletz, T. & Driever, W. Zeb1 regulates E-cadherin and Epcam (epithelial cell adhesion molecule) expression to control cell behavior in early zebrafish development. *J. Biol. Chem.* **288,** 18643–18659 (2013).
23. Dosch, J. S., Ziemke, E. K., Shettigar, A., Rehemtulla, A. & Sebolt-Leopold, J. S. Cancer stem cell marker phenotypes are reversible and functionally homogeneous in a preclinical model of pancreatic cancer. *Cancer Res.* **75,** 4582–4592 (2015).
24. Wellner, U. *et al.* The EMT-activator ZEB1 promotes tumorigenicity by repressing stemness-inhibiting microRNAs. *Nat. Cell Biol.* **11,** 1487–1495 (2009).
25. Herreros-Villanueva, M. *et al.* SOX2 promotes dedifferentiation and imparts stem cell-like features to pancreatic cancer cells. *Oncogenesis* **2,** e61 (2013).
26. Sanada, Y. *et al.* Histopathologic evaluation of stepwise progression of pancreatic carcinoma with immunohistochemical analysis of gastric epithelial transcription factor SOX2: comparison of expression patterns between invasive components and cancerous or nonneoplastic intraductal components. *Pancreas* **32,** 164–170 (2006).
27. Singh, S. K. *et al.* Antithetical NFATc1–Sox2 and p53–miR200 signaling networks govern pancreatic cancer cell plasticity. *EMBO J.* **34,** 517–530 (2015).
28. Muller, P. A. J. & Vousden, K. H. Mutant p53 in cancer: new functions and therapeutic opportunities. *Cancer Cell* **25,** 304–317 (2014).
29. Rivlin, N., Koifman, G. & Rotter, V. p53 orchestrates between normal differentiation and cancer. *Semin. Cancer Biol.* **32,** 10–17 (2015).

30. Morton, J. P. *et al*. Mutant p53 drives metastasis and overcomes growth arrest/senescence in pancreatic cancer. *Proc. Natl Acad. Sci. USA* **107,** 246–251 (2010).
31. Lehmann, W. *et al*. ZEB1 turns into a transcriptional activator by interacting with YAP1 in aggressive cancer types. *Nat. Commun.* **7,** 10498 (2016).
32. Mock, K. *et al*. The EMT-activator ZEB1 induces bone metastasis associated genes including BMP-inhibitors. *Oncotarget* **6,** 14399–14412 (2015).
33. Brabletz, S. *et al*. The ZEB1/miR-200 feedback loop controls Notch signalling in cancer cells. *EMBO J.* **30,** 770–782 (2011).
34. Singh, A. *et al*. A gene expression signature associated with "K-Ras addiction" reveals regulators of EMT and tumor cell survival. *Cancer Cell* **15,** 489–500 (2009).
35. Nakamura, T., Fidler, I. J. & Coombes, K. R. Gene expression profile of metastatic human pancreatic cancer cells depends on the organ microenvironment. *Cancer Res.* **67,** 139–148 (2007).
36. Collisson, E. A. *et al*. Subtypes of pancreatic ductal adenocarcinoma and their differing responses to therapy. *Nat. Med.* **17,** 500–503 (2011).
37. Weissmueller, S. *et al*. Mutant p53 drives pancreatic cancer metastasis through cell-autonomous PDGF receptor β signaling. *Cell* **157,** 382–394 (2014).
38. Diepenbruck, M. & Christofori, G. Epithelial–mesenchymal transition (EMT) and metastasis: yes, no, maybe? *Curr. Opin. Cell Biol.* **43,** 7–13 (2016).
39. Ye, X. & Weinberg, R. A. Epithelial–mesenchymal plasticity: a central regulator of cancer progression. *Trends Cell Biol.* **25,** 675–686 (2015).
40. Bellomo, C., Caja, L. & Moustakas, A. Transforming growth factor [beta] as regulator of cancer stemness and metastasis. *Br. J. Cancer* **115,** 761–769 (2016).
41. Korpal, M. & Kang, Y. Targeting the transforming growth factor-β signalling pathway in metastatic cancer. *Eur. J. Cancer* **46,** 1232–1240 (2010).
42. Lehuédé, C., Dupuy, F., Rabinovitch, R., Jones, R. G. & Siegel, P. M. Metabolic plasticity as a determinant of tumor growth and metastasis. *Cancer Res.* **76,** 5201–5208 (2016).
43. Nieto, M. A. Epithelial plasticity: a common theme in embryonic and cancer cells. *Science* **342,** 1234850 (2013).
44. Brabletz, T. *et al*. Variable beta-catenin expression in colorectal cancer indicates a tumor progression driven by the tumor environment. *Proc. Natl Acad. Sci. USA* **98,** 10356–10361 (2001).
45. Chaffer, C. L. *et al*. Normal and neoplastic nonstem cells can spontaneously convert to a stem-like state. *Proc. Natl Acad. Sci. USA* **108,** 7950–7955 (2011).
46. Puisieux, A., Brabletz, T. & Caramel, J. Oncogenic roles of EMT-inducing transcription factors. *Nat. Cell Biol.* **16,** 488–494 (2014).
47. Chaffer, C. L. *et al*. Poised chromatin at the ZEB1 promoter enables breast cancer cell plasticity and enhances tumorigenicity. *Cell* **154,** 61–74 (2013).
48. Gruber, R. *et al*. YAP1 and TAZ control pancreatic cancer initiation in mice by direct up-regulation of JAK–STAT3 signaling. *Gastroenterology* **151,** 526–539 (2016).
49. Zhang, W. *et al*. Downstream of mutant KRAS, the transcription regulator YAP Is essential for neoplastic progression to pancreatic ductal adenocarcinoma. *Sci. Signal.* **7,** ra42-ra42 (2014).
50. Moffitt, R. A. *et al*. Virtual microdissection identifies distinct tumor- and stroma-specific subtypes of pancreatic ductal adenocarcinoma. *Nat. Genet.* **47,** 1168–1178 (2015).
51. Galvan, J. A. *et al*. Expression of E-cadherin repressors SNAIL, ZEB1 and ZEB2 by tumour and stromal cells influences tumour-budding phenotype and suggests heterogeneity of stromal cells in pancreatic cancer. *Br. J. Cancer* **112,** 1944–1950 (2015).
52. Bronsert, P. *et al*. Prognostic significance of Zinc finger E-box binding homeobox 1 (ZEB1) expression in cancer cells and cancer-associated fibroblasts in pancreatic head cancer. *Surgery* **156,** 97–108 (2014).
53. Singh, A. & Settleman, J. EMT, cancer stem cells and drug resistance: an emerging axis of evil in the war on cancer. *Oncogene* **29,** 4741–4751 (2010).
54. Eser, S., Schnieke, A., Schneider, G. & Saur, D. Oncogenic KRAS signalling in pancreatic cancer. *Br. J. Cancer* **111,** 817–822 (2014).
55. Ni, T. *et al*. Snail1-dependent p53 repression regulates expansion and activity of tumour-initiating cells in breast cancer. *Nat. Cell Biol.* **18,** 1221–1232 (2016).
56. Turajlic, S. & Swanton, C. Metastasis as an evolutionary process. *Science* **352,** 169–175 (2016).
57. Caramel, J. *et al*. A switch in the expression of embryonic EMT-inducers drives the development of malignant melanoma. *Cancer Cell* **24,** 466–480 (2013).
58. Denecker, G. *et al*. Identification of a ZEB2-MITF-ZEB1 transcriptional network that controls melanogenesis and melanoma progression. *Cell Death Differ.* **21,** 1250–1261 (2014).
59. Ye, X. *et al*. Distinct EMT programs control normal mammary stem cells and tumour-initiating cells. *Nature* **525,** 256–260 (2015).
60. Tiwari, N. *et al*. Sox4 is a master regulator of epithelial-mesenchymal transition by controlling Ezh2 expression and epigenetic reprogramming. *Cancer Cell* **23,** 768–783 (2013).
61. Tran, H. D. *et al*. Transient SNAIL1 expression is necessary for metastatic competence in breast cancer. *Cancer Res.* **74,** 6330–6340 (2014).

METHODS

Ethics statement. Animals were kept on a 12:12 h light–dark cycle and provided with food and water *ad libitum*. Animal husbandry and all experiments were carried out according to the European Animal Welfare laws and guidelines. The protocols were approved by the committee on ethics of animal experiments of the states Baden-Württemberg and Bavaria (Regierungspräsidium Freiburg and Regierung Unterfranken, Würzburg).

Mice. The *Pdx1-Cre* transgene (Tg(Pdx1-cre)6Tuv), the conditional *Kras*$^{LSL.G12D}$ (Kras^{tm4Tyj}), *Tp53*$^{LSL.R172H}$ (Trp53^{tm2Tyj}) and GFP (Z/EG; Tg(CAG-Bgeo/GFP)21Lbe) alleles and the KPC mouse model have been described[9,62–66], and were kept on a C57BL/6 background. The generation of the conditional *Zeb1* knockout allele (*Zeb1*^{fl}) is described elsewhere[12]. In brief, exon 6 was flanked by loxP sites to remove sequences coding for large parts of the protein and to induce a premature translational stop. Tumour mice were generated by breeding *Pdx1-Cre* with *Kras*$^{LSL.G12D/+}$;*Tp53*$^{LSL.R172H/+}$ mice (KPC) and *Pdx1-Cre;Zeb1*$^{fl/fl}$ with *Kras*$^{LSL.G12D/+}$;*Tp53*$^{LSL.R172H/+}$;*Zeb1*$^{fl/fl}$ mice (KPCZ). KPC and KPCZ offspring were palpated weekly for tumour initiation and enrolled for MRI measurements when tumours were identified. KC and KCZ mice (*Tp53*$^{+/+}$ genotype) were analysed at 6 months of age. Once the tumour reached a maximum tolerated size (tumour diameter of 1 cm), mice were killed and perfused, and organs, tumour and macroscopic metastases were isolated. Animals that died or were killed for reasons other than pancreatic tumours (mainly growth of skin papilloma) were excluded from the analyses. Tissue was fixed in 4% paraformaldehyde (PFA) or snap frozen in Tissue-Tek. A summary of basic tumour mouse data is shown in Supplementary Table 1.

MRI. Mice were analysed with a Bruker BioSpin 94/20, 9.4 Tesla—400 MHz—20 cm small-animal MR using coronal and transverse scans with a spatial resolution of 117 μm × 117 μm/pixel and a 256 × 256 matrix. Slice distance was set to 0.5 mm. Measurements were repeated weekly. Tumour volume was approximated by $\pi/6lwd$. Initial detection of a tumour after a series of tumour-free MRI measurements was defined as the time of tumour initiation. For analysis of tumour growth curves all mice were adjusted to a tumour size of 50 mm^3.

Histology, histopathology and immunohistochemistry. PFA-fixed tissues were embedded in paraffin, sectioned at 4–5 μm and stained with Mayer's haematoxylin and eosin solution G (HE). For histopathological scoring, tumours were classified using the standard pathological grading scheme into either well differentiated (grade 1), moderately differentiated (grade 2), poorly differentiated (grade 3) or anaplastic or sarcomatoid (grade 4). The histological invasion score was scored from no invasion (0) to high invasion (2), with invasion defined as number and distance of tumour cells disseminated from the main tumour mass. Masson's trichrome staining (MTS) was carried out according to the manufacturer's instructions (Sigma-Aldrich, HT15) and counterstained with Weigert's iron haematoxylin. Tumour stroma composition was scored on the basis of either MTS or HE staining for intensity of extracellular matrix deposition on a scale from 0 to 4. KC and KCZ pancreata were stained with alcian blue–PAS reagent. Scoring for CD31 and Gata6 was done according to staining intensity, with no (0), low (1), medium (2) and high (3) expression. PanINs were classified using the standard pathological grading score from 1 to 3. The total numbers of PanINs and ADMs were counted on at least four independent tumour sections and normalized to a tissue area of 20 mm^2. In addition to macroscopic metastases, lungs and livers were screened for metastases, identified by screening four series of HE-stained sections separated by at least 200 μm.

Immunohistochemical analysis was carried out as previously described[31]. The following primary antibodies were used: polyclonal rabbit anti-Zeb1 (Novus Biological, NBP1-05987, 1:250); polyclonal rabbit anti-Zeb2 (Novus Biological, NBP1-82991, 1:200); monoclonal rabbit anti-Snail (Cell Signaling, no. 3879, clone C15D3, 1:200); monoclonal rabbit anti-Slug (Cell Signaling, CS9585, Clone C19G7, 1:150); polyclonal goat anti-Twist (Abcam, ab50581, 1:500); polyclonal goat anti-Gata6 (R&D, AF1700, 1:1,500); monoclonal mouse anti-E-cadherin (BD Transduction Laboratories, 610182, clone 36, 1:350); monoclonal rabbit anti-CD31 (Santa Cruz, sc-1506, clone M-20, 1:50); monoclonal rabbit anti-Ki67 (Abcam, ab16667, clone SP6, 1:300); monoclonal rabbit anti-cleaved caspase 3 (Cell Signaling, CS9664, clone 5A1E, 1:1,000); monoclonal rat anti-KRT19 (TROMA-3 hybridoma supernatant,1:20, gift from Rolf Kemler); polyclonal rabbit anti-Sox2 (Abcam, ab97959, 1:1,000). These were counterstained with Mayer's haematoxylin. For Zeb1 immunofluorescence staining, cryosections were fixed in 4% PFA for 10 min, then permeabilized for 10 min in 0.25% Triton X-100/PBS. After blocking in 3% BSA/PBS, tissue was incubated with anti-Zeb1 antibody (Sigma, HPA027524, 1:100) followed by Alexa594-conjugated secondary antibody (Life Technologies). All images were acquired on a Leica DM5500B microscope and a 2D deconvolution was carried out when appropriate. No statistical method was used to predetermine sample size and the experiments were not randomized. Histological analyses were carried out by two independent pathologists. The investigators were not blinded to allocation during experiments or outcome assessment. Each demonstrated immunohistochemical and immunofluorescent image was representative of five or more cases (tumours) of the indicated subtype.

Primary cell lines. A small piece of primary tumour was dissected, minced with a scalpel and plated on six-well plates in DMEM (Gibco, 31966)/10% fetal bovine serum (Gibco, 10500)/1% penicillin/streptomycin (Gibco, 15140) at 37 °C/5% CO_2 in a humidified incubator. Tumour cells that attached to the plate and grew out were passaged for generation of cell lines. Successful and complete recombination of cell-line deprivation was confirmed by PCR. KPCS cells were obtained from D. Saur (Department of Internal Medicine, TU Munich, Germany) and generated from the same KPC mouse model that additionally carried a homozygous *Snai1* deletion[67]. For partial knockdown of *Zeb1*, cells were infected with lentivirus containing a pGIPZ shZeb1 knockdown (V2LMM_18639) or a pGIPZ non-silencing shRNA control construct. Puromycin-resistant GFP medium/high cells were used. Zeb1 protein expression was normalized to β-actin levels using BioRad Image Lab Software to calculate knockdown efficiencies. Induction of EMT in primary tumour cell lines was carried out by adding 5 ng ml^{-1} TGFβ1 (PeproTech, 100-21) and replacing the medium daily for the duration of the experiment. MicroRNA overexpression was carried out as previously described[31]. For FACS analysis of cancer stem cells markers 1×10^6 cells were incubated with a combination of monoclonal rat anti-CD24-PE (BD, 553262, clone M1/69, 1:200), monoclonal rat anti-CD44-APC (BD, 561862, clone IM7, 1:100) and monoclonal rat anti-EpCAM-FITC (ebioscience, 11-5791, clone G8.8, 1:200) antibodies and analysed in a BD Cytoflex using CytExpert software. A total of 10,000 vital cells were counted. All studies were carried out on cells cultured for fewer than 30 passages. All experiments using primary cells *in vitro* were done at least in triplicate ($n = 3$). Only primary cells from mouse tumours were used, and these were not further authenticated or tested for mycoplasma contamination.

Immunoblotting, RNA isolation and quantitative RT-PCR. Protein was extracted with RIPA buffer and western blotting was carried out as described[31,32], with the exception that protein detection on the nitrocellulose membrane was done using incubation in Western Lightning Plus-ECL (Perkin Elmer, NEL103001EA) or SuperSignal West Femto Maximum Sensitivity Substrate (Thermo Scientific, 34095) and a ChemiDoc imaging system (BioRad). Antibodies against the following proteins were used: polyclonal rabbit anti-Zeb1 (Sigma, HPA027524, 1:5,000); monoclonal rabbit anti-Snail (Cell Signaling, no. 3879, clone C15D3, 1:1,000); monoclonal mouse anti-E-cadherin (BD Transduction Laboratories, 610182, clone 36, 1:5,000); monoclonal mouse anti-N-cadherin (BD Transduction Laboratories, 610920, clone 32, 1:1,000); monoclonal rabbit anti-vimentin (Cell Signaling, CS5741, clone D21H3, 1:5,000); monoclonal mouse anti-β-actin (Sigma, A5441, clone AC-15, 1:10,000); polyclonal rabbit anti-Sox2 (Novus Biological, NB110-37235, 1:3,000); monoclonal mouse anti-Bmi1 (Millipore, 05-673, clone F6, 1:300); monoclonal rabbit anti-PDGFRβ (Cell Signaling, CS3169, clone 28E1, 1:1,000); monoclonal rabbit anti-Sparc (Cell Signaling, CS8725; Clone D10F10, 1:1,000); monoclonal mouse anti-α-tubulin (Sigma, T6199, clone DM1A, 1:5,000). Western blots were done for at least three individual experiments and one representative blot is shown.

Total RNA was isolated and reversely transcribed using the RNeasy Plus Mini Kit (Qiagen, 74136) and the RevertAid First Strand cDNA Synthesis Kit (Thermo, K1622) for mRNA and the miRCURY universal cDNA synthesis kit II (Exiqon, 203301) for microRNA. mRNA transcripts were detected using complementary DNA from 7.5 ng total RNA with 300 nM gene-specific primers, the Universal Probe Library (Roche, 04869877001) and the TaqMan Universal Master Mix (4440040, Applied Biosystems) in a 12 μl volume. MicroRNAs were analysed with the miRCURY ExiLENT SYBR Green Kit (Exiqon, 203421) with specific primer sets (Exicon) according to the manufacturer's instructions. All samples were run in a LightCycler 480 (Roche) and values were normalized to *Gapdh* and *Mir16-1* levels where appropriate and expressed relative to controls. For primer sequences and miR primer set details see Supplementary Table 3.

Cell viability (MTT) and BrdU cell proliferation assays. Cell viability on gemcitabine (Sigma, G6423; ranging from 0.78 to 1,000 nM) and erlotinib treatment (Cell Signaling, 5083, or Selleckchem, S1023, ranging from 0.2 to 51.2 μM) was analysed by plating 6,000 cells in 96- or 48-well plates and measured after 72 h of treatment using 5 mg ml^{-1} MTT (methylthiazolyldiphenyl-tetrazolium bromide; Sigma, M2128) as described[68]. IC50 values were calculated with GraphPad Prism using logarithm-transformed data and non-linear regression. For proliferation analysis 1,000 cells were plated in 96-well plates and BrdU incorporation was measured after a 2 h pulse with BrdU using the Cell Proliferation ELISA Kit (Roche, 11647229001) according to the manufacturer's instructions.

Sphere assay. To detect sphere-forming capacity, cells were resuspended as single-cell suspensions in serum-free DMEM/F12 medium (Gibco, 31331), containing 1%

DOI: 10.1038/ncb3513

methylcellulose (Sigma, M0512), 20 ng ml^{-1} human epidermal growth factor (R&D Systems, 236-EG), 20 ng ml^{-1} human fibroblast growth factor (BD Biosciences, 354060), B27 supplement (1:50, Invitrogen, 17504), N2 supplement (1:100, Gibco, 17502) and 1% penicillin/streptomycin. 500 single cells were seeded into individual wells of poly(2-hydroxyethylmethacrylate)-coated (Sigma, P3932) 96-well plates. Colonies with a diameter of more than 80 μm were counted after 12 days.

Immunofluorescence staining. Immunofluorescence labelling was carried out as described previously[31]. Cells were seeded on coverslips and fixed with 4% PFA, followed by permeabilization with 0.1% Triton X-100/PBS. After blocking in 3% BSA/PBS, cells were incubated with primary antibodies overnight at 4 °C (polyclonal rabbit anti-Zeb1 (Sigma, HPA027524, 1:300); monoclonal mouse anti-E-cadherin (BD Transduction Laboratories, 610182, clone 36, 1:200)), followed by appropriate Alexa594- and Alexa488-conjugated secondary antibodies (Life Technologies) for 1 h at RT. All images were acquired with a Leica DM5500B microscope and the LAX software (Leica). All immunofluorescence experiments were carried out in at least three individual experiments and one representative image is shown.

Lung colonization/tumorigenicity. Tumour-cell colonization and metastasizing capacities to the lung were analysed by tail-vein injections into syngeneic mice or NMRI-*Foxn1*$^{nu/nu}$ mice. Primary tumour cell lines were trypsinized and resuspended in appropriate volumes of PBS to inject 200,000 tumour cells in a 200 μl volume using a 27G needle. Mice were killed after 18 days and analysed for lung metastasis by HE staining. For each cell line three mice were injected and the number of lung metastases was counted in two independent sections separated by at least 200 μm. For short-term colonization analysis cells were infected with pCDH-MSCV-LUC_EF1-GFP-T2A-Puro, selected by puromycin and sorted for medium to high levels of GFP expression. Mice were killed 2 h after tail-vein injection. To calculate tumorigenicity and analysis of tumour growth on subcutaneous engraftment 500, 2,500, 12,500 and 100,000 cells were injected into the flanks of C57BL/6 mice. Tumour size was measured three times per week and mice were killed if tumours exceeded the size of 500 mm^3 or ulcerated. Tumour-initiating frequencies were calculated using the ELDA software (http://bioinf.wehi.edu.au/software/elda).

Microarray analysis, pre-processing, GSEA and data availability. Gene expression of three epithelial and three mesenchymal KPC, six KPCZ, two TGFβ-treated epithelial KPC and two TGFβ-treated KPCZ cell lines was measured using Illumina Mouse WG6 v2 BeadArrays (Illumina). Total RNA was isolated, labelled and hybridized according to the manufacturer's protocol in two separate experiments. Raw microarray data were processed and quantile normalized using the Bioconductor R package beadarray[69] and subsequently batch corrected according to their chip identity through ComBat[70] as implemented in the R Bioconductor sva package. Illumina probes were mapped to Entrez IDs using the IlluminaMousev2 annotation (v. 1.26) from Bioconductor. If several probes mapped to the same Entrez ID, the one having the largest interquartile range was retained, which resulted in 20,052 uniquely annotated genes. GSEA was carried out using the Broad Institute platform (http://www.broadinstitute.org/gsea/index.jsp; version 2.2.2). A total of 189 gene sets of the oncogenic signature C6 from the Molecular Signatures database (http://www.broadinstitute.org/gsea/msigdb/genesets.jsp?collection=C6) were used for the analysis with default settings and 1,000 gene set permutations. An additional 36 gene sets, related to pancreatic cancer, Zeb1 or metastasis, were selected from MSigDB and also analysed (Supplementary Table 4). Gene sets from classical, quasi-mesenchymal and exocrine-like PDAC subtypes were obtained from the authors of ref. 36.

Metabolic parameters. Bioenergetics of epithelial KPC and KPCZ cell lines was determined using an XFe96 Extracellular Flux Analyzer (Seahorse Bioscience/Agilent Technologies). Cells were seeded in specialized cell-culture microplates at a density of 15,000/well and cultured for 18 h. 1 h before the measurement, cells were incubated at 37 °C in a CO_2-free atmosphere. For the determination of glycolytic parameters a glucose stress test was carried out: basal ECAR (indicative of glycolysis) was first determined under glucose-free conditions. Second, the rate of glycolysis was calculated using the ECAR after glucose supplementation (10 mM). Finally, glycolytic capacity and glycolytic reserve were calculated after inhibition of mitochondrial respiration through oligomycin (Sigma, 75351, 1 μM) and hexokinase activity through 2-deoxy-glucose (2DG, Sigma, D6134, 100 mM). For the determination of respiratory parameters a mitochondrial stress test was carried out: basal OCR (indicator for mitochondrial respiration) was measured. Next, responses to the subsequent addition of oligomycin (1 μM), carbonyl cyanide 4-(trifluoromethoxy)phenylhydrazone (Sigma, C2920, 1 μM) and a combination of antimycin A (Sigma, A8674, 3 μM) and rotenone (Sigma, R8875, 3 μM) were evaluated, allowing for calculation of basal and maximal respiration as well as respiration-related ATP production. All experiments were carried out in heptaplicates.

Statistics and reproducibility. Statistical analysis was carried out using GraphPad Prism software (version 6.07). Data are represented by means ± s.d. unless otherwise indicated. For survival analysis the log-rank Mantel–Cox test was used. Tumour/PanIN grading, extracellular matrix (ECM) deposition, local invasion, CD31 and Gata 6 staining, Ki67-positive tumour-cell counting, cleaved Casp3-positive tumour-cell numbers, PanIN areas, lung-colonization assay and sphere-forming capacity were tested for significance with a two-tailed Mann–Whitney test or an unpaired two-tailed *t*-test as indicated. Welch's correction was carried out where appropriate. Chi-square analysis was carried out to compare frequency of metastases and number of tumour-initiating cells as well as frequency of Zeb1, Snail, Slug, Twist Zeb2, E-cad and Sox2 positive tumours. Tumour growth, ECAR and OCR were tested for significance at individual times by a *t*-test with a Holm–Sidak test for multiple comparison. qPCR data were tested for significance with a one-tailed Mann–Whitney test or an unpaired one-tailed *t*-test as indicated. *P*-values of statistical significance are represented as $^{*}P < 0.05$; $^{**}P < 0.01$; $^{***}P < 0.001$; $^{****}P < 0.0001$.

Data availability. Microarray data generated in this study have been deposited in the Gene Expression Omnibus (GEO) under accession code GSE87472. The 189 publicly available gene sets reanalysed here were from of the oncogenic signature C6 available from the Molecular Signatures database (http://www.broadinstitute.org/gsea/msigdb/genesets.jsp?collection=C6, Broad Institute, 741 MSigDB, version 5.1). The 36 publicly available gene sets related to pancreatic cancer, Zeb1 or metastasis were selected from MSigDB and reanalysed here (see also Supplementary Table 4). Gene sets from classical, quasi-mesenchymal and exocrine-like PDAC subtypes reanalysed here were obtained from the authors of ref. 36.

Source data for Figs 3c,d,f and 6d,g and Supplementary Figs 5d and 7a have been provided as Supplementary Table 5. All other data supporting the findings of this study are available from the corresponding author on reasonable request.

62. Olive, K. P. *et al.* Mutant p53 gain of function in two mouse models of Li-Fraumeni syndrome. *Cell* **119,** 847–860 (2004).
63. Jackson, E. L. *et al.* Analysis of lung tumor initiation and progression using conditional expression of oncogenic K-ras. *Genes Dev.* **15,** 3243–3248 (2001).
64. Hingorani, S. R. *et al.* Preinvasive and invasive ductal pancreatic cancer and its early detection in the mouse. *Cancer Cell* **4,** 437–450 (2003).
65. Chan, I. T. *et al.* Conditional expression of oncogenic K-ras from its endogenous promoter induces a myeloproliferative disease. *J. Clin. Invest.* **113,** 528–538 (2004).
66. Novak, A., Guo, C., Yang, W., Nagy, A. & Lobe, C. G. Z/EG, a double reporter mouse line that expresses enhanced green fluorescent protein upon Cre-mediated excision. *Genesis* **28,** 147–155 (2000).
67. Murray, S. A., Carver, E. A. & Gridley, T. Generation of a Snail1 (Snai1) conditional null allele. *Genesis* **44,** 7–11 (2006).
68. Meidhof, S. *et al.* ZEB1-associated drug resistance in cancer cells is reversed by the class I HDAC inhibitor mocetinostat. *EMBO Mol. Med.* **7,** 831–847 (2015).
69. Dunning, M. J., Smith, M. L., Ritchie, M. E. & Tavare, S. beadarray: R classes and methods for Illumina bead-based data. *Bioinformatics* **23,** 2183–2184 (2007).
70. Johnson, W. E., Li, C. & Rabinovic, A. Adjusting batch effects in microarray expression data using empirical Bayes methods. *Biostatistics* **8,** 118–127 (2007).

nature cell biology

DOI: 10.1038/ncb3513

In the format provided by the authors and unedited.

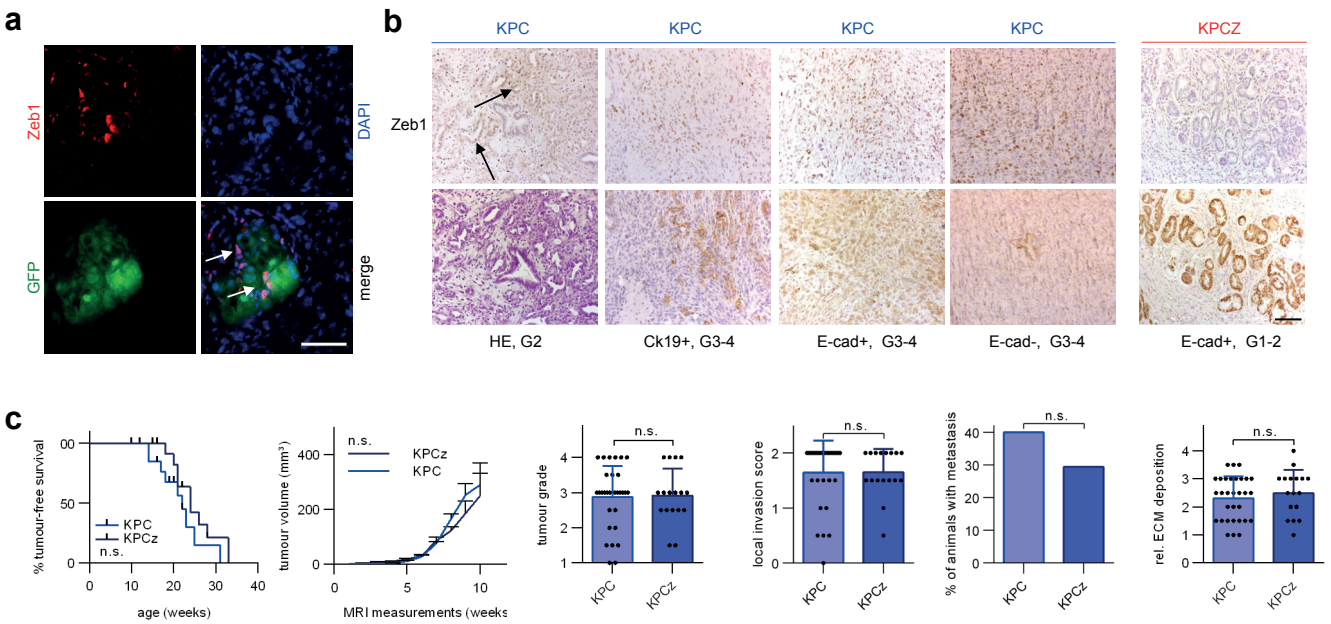

Supplementary Figure 1 Characterisation of KPC, heterozygously and homozygously *Zeb1* depleted KPC tumours. **(a)** Representative Zeb1-immunolabeling of a GFP lineage-traced primary tumour showing Zeb1/GFP double-positive tumour cells (arrows). n=5 independent tumors. Scale bar, 50 µm. **(b)** Representative consecutive sections of HE and indicated immunohistochemical stainings of four Zeb1 expressing KPC tumours demonstrating the heterogeneity in phenotype, grading and marker expression. A representative differentiated Zeb1-negative KPCZ tumour is shown for comparison. Arrows indicate Zeb1 positive tumour cells in the differentiated KPC tumour. n= 15 KPC, 13 KPCZ independent tumours. Scale bar, 100 µm. **(c)** Tumour-free survival of KPC mice vs. KPC mice with a heterozygous deletion of *Zeb1* (KPCz) (n= 15 KPC, 16 KPCz independent tumours); log-rank (Mantel-Cox) test); tumour volume (0 = start of MRI measurements, n=12 KPC, 14 KPCz independent tumours); error bars show mean ±S.E.M.; multiple t-tests with correction for multiple comparison using the Holm-Sidak method; grading, local invasion and relative ECM deposition of the respective tumours (n=31 KPC, 17 KPCz; Mann-Whitney test (two-tailed); percentage of metastasized tumours (n=35 KPC, 17 KPCz independent tumours; Chi-square test (two-tailed); n.s. = not significant.

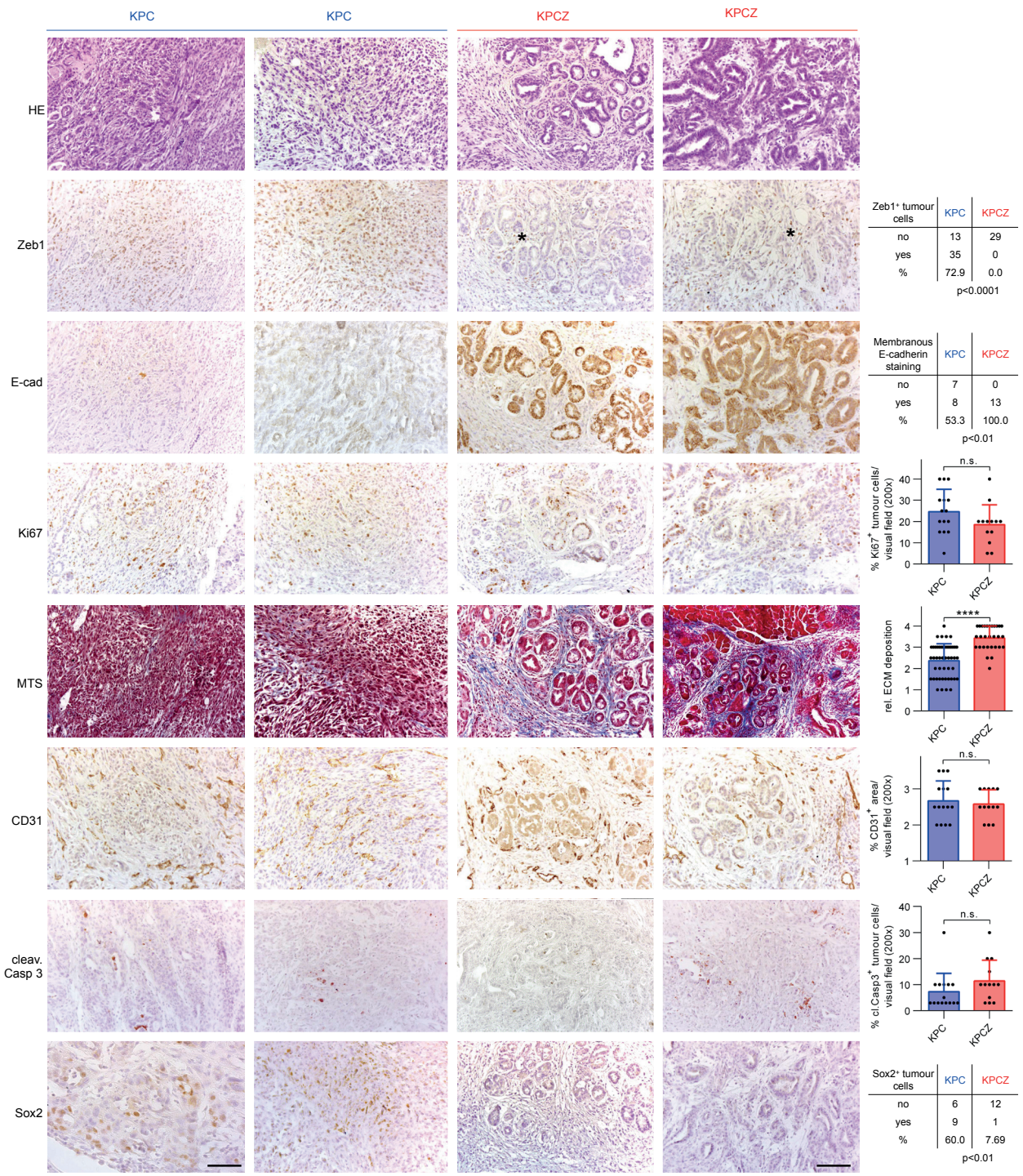

Supplementary Figure 2 Characterisation of KPC vs. KPCZ tumours. Representative images of immunohistochemical and histological stainings of KPC and KPCZ tumours and quantifications of the indicated markers are given. Asterisks label Zeb1-expressing stroma cells in KPCZ tumours. Specific blue MTS staining labels collagen fibres. Scale bars, 100 μm, for lower left image 50 μm. n=48 KPC, 29 KPCZ independent tumours for Zeb1 and MTS; n= 15 independent tumours for KPC, 13 independent tumours for KPCZ for all other markers, error bars show mean ±S.D.; ****p<0.0001, n.s. = not significant, Chi-square test (two-tailed) for Zeb1, E-cadherin and Sox2, unpaired Student's t-test (two-tailed) for Ki67 and Casp3 (with Welch's correction), Mann-Whitney test (two-tailed) for ECM and CD31.

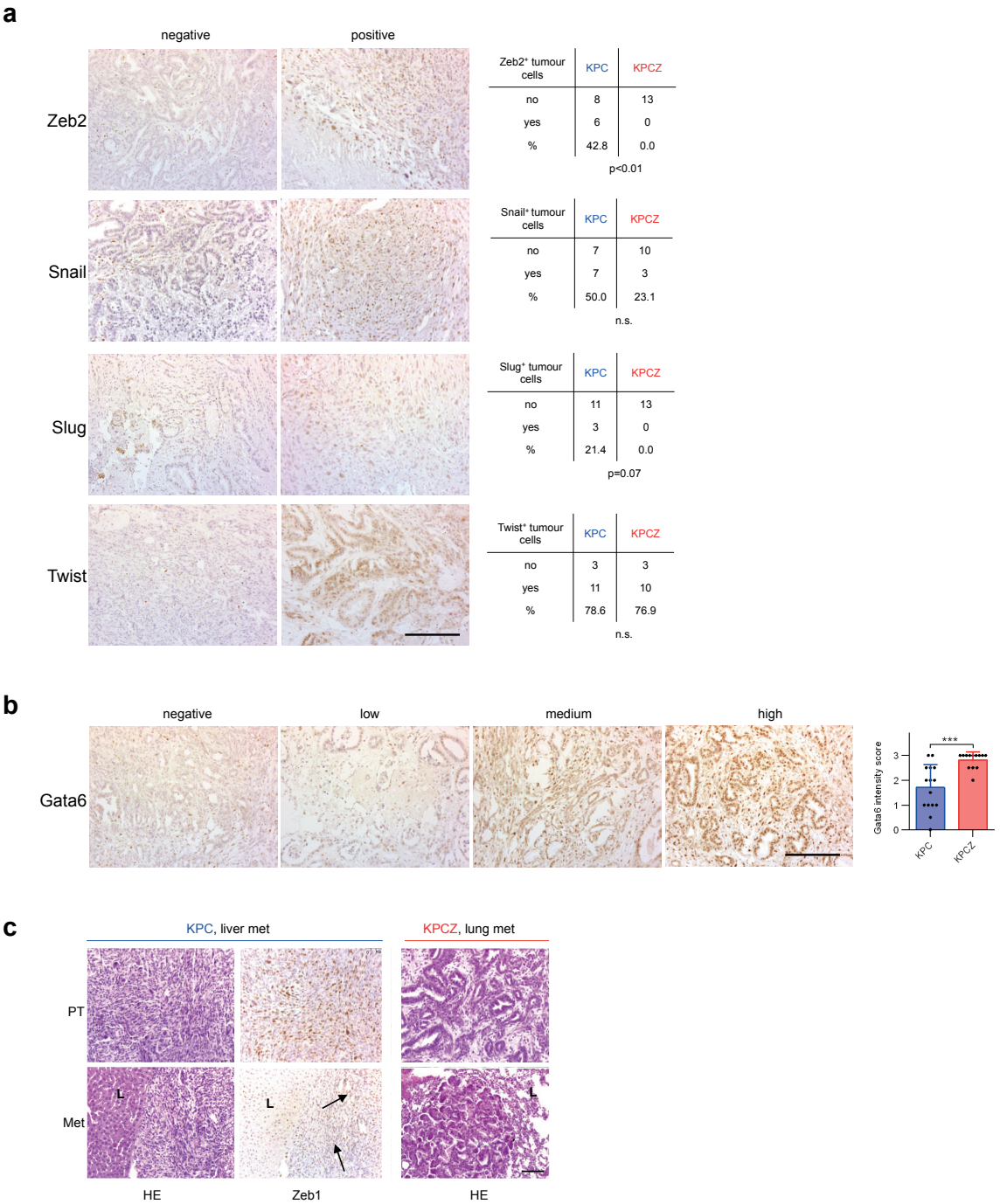

Supplementary Figure 3 Characterisation of differentiaton markers in KPC vs. KPCZ tumours. **(a)** Representative images of positive and negative immunohistochemical stainings and statistical analysis for the indicated EMT-TFs. Scale bar, 150 μm. n= 14 independent tumours for KPC, 13 independent tumours for KPCZ, Chi-square test (two-tailed); n.s. = not significant. **(b)** Representative images of immunohistochemical stainings and statistical analysis for expression of Gata6. Scale bar, 150 μm. n=14 independent tumours for KPC, 13 independent tumours for KPCZ; error bars show mean ±S.D.; Mann-Whitney test (two-tailed), ***p<0.001. **(c)** Representative images of differentiated KPCZ and undifferentiated KPC primary tumours (PT) and corresponding metastases (Met) with the same phenotype. Immunohistochemical labelling of Zeb1 expressing tumour cells in the KPC PT and Met (arrows). L= liver or lung tissue. n= 19 KPC, 4 KPCZ independent tumours and corresponding metastases. Scale bar, 100 μm.

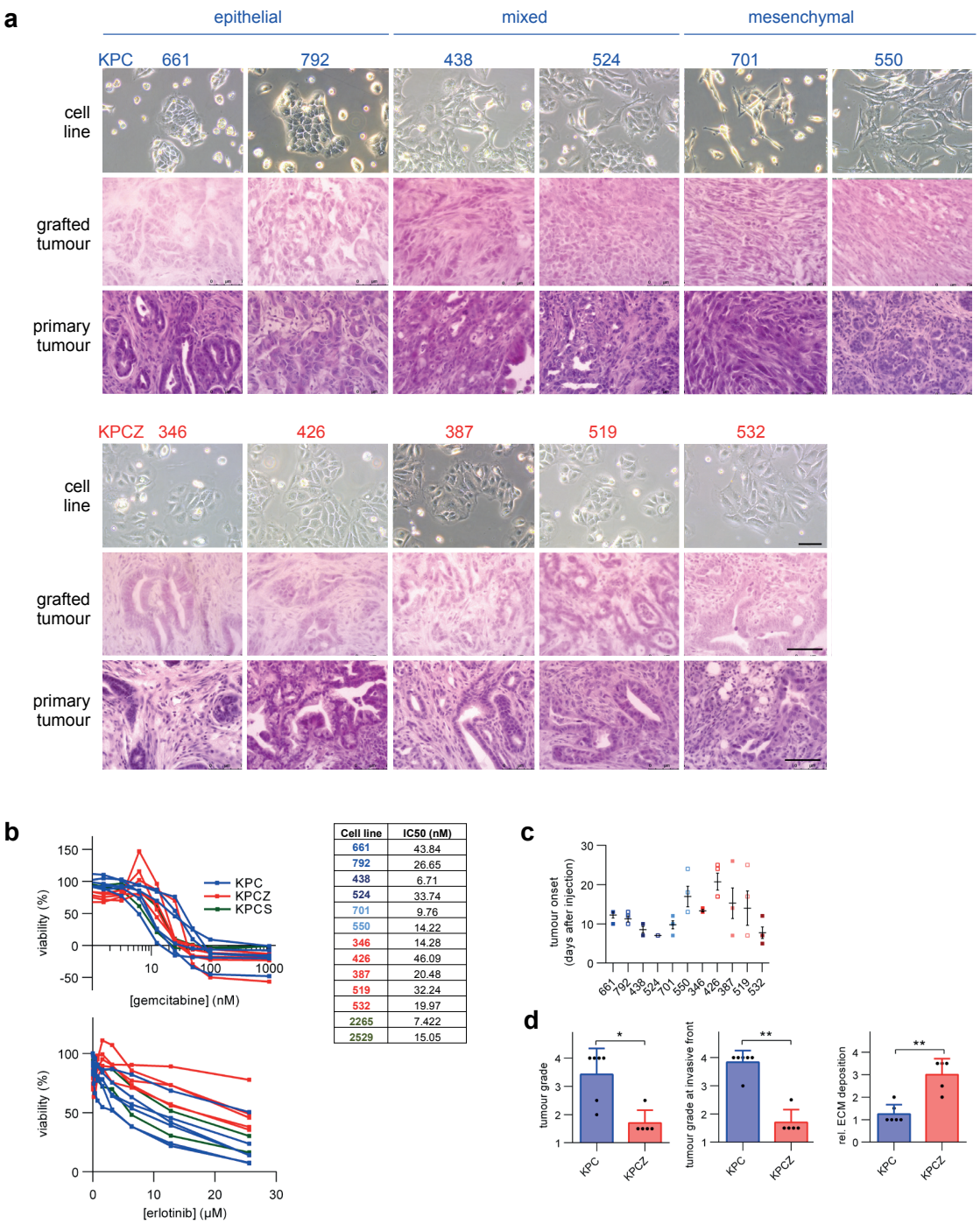

Cell line	IC50 (nM)
661	43.84
792	26.65
438	6.71
524	33.74
701	9.76
550	14.22
346	14.28
426	46.09
387	20.48
519	32.24
532	19.97
2265	7.422
2529	15.05

Supplementary Figure 4 Characterisation of KPC vs. KPCZ tumour derived cell lines. **(a)** Bright field image of primary cell lines from KPC and KPCZ tumours as well as HE stainings of the respective tumours after grafting in syngeneic mice and of the respective primary tumours are shown. Scale bars, 100 μm for bright field, 75 μm for HE stainings. **(b)** MTT viability assay for the isolated tumour cell lines after treatment with the indicated doses of gemcitabine and erlotinib. The calculated IC50 values for gemcitabine are shown. n=3 biologically independent experiments, error bars show mean ±S.E.M. **(c)** Tumour onset after subcutaneous injection of 1 x 10^5 KPC and KPCZ cells into syngeneic mice. n=4 mice/cell line, error bars show mean ±S.E.M. **(d)** Tumour grading, grading at invasive regions and relative ECM deposition of one representative tumour/cell line analysed in c) (n=6 tumours for KPC, n=5 tumours for KPCZ); error bars show mean ±S.D.; *p<0.05, **p<0.01, Mann-Whitney test (two-tailed).

a

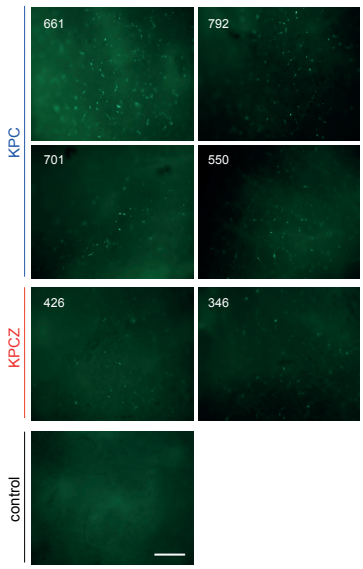

b

	500 cells	2500 cells	12500 cells	Stem cell fraction
661	1/4	3/4	4/4	1/ 1773
792	1/4	3/4	7/8	1/ 4012
438	2/4	0/4	4/4	1/ 4300
524	3/4	2/4	6/8	1/ 5210
550	0/4	1/4	3/6	1/16143
701	0/4	2/4	1/4	1/17484
532	0/4	2/4	3/4	1/17700
346	0/4	0/4	2/4	1/24215
426	0/4	0/4	1/4	1/55516
519	0/4	0/4	1/4	1/55516
387	0/4	0/4	0/4	Inf

all KPC vs KPCZ cell lines $p < 0.0001$ (****)

c

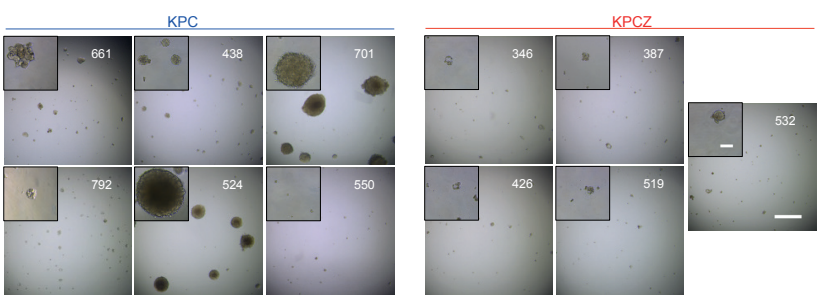

d

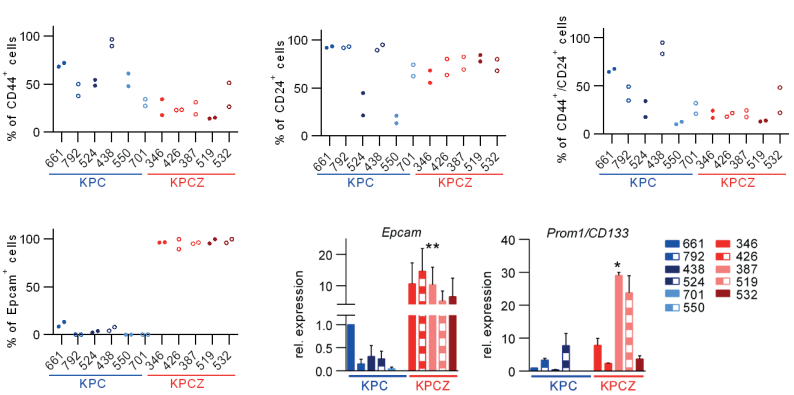

Supplementary Figure 5 Depletion of *Zeb1* affects tumour promoting capacities. **(a)** Representative images of one visual field (n=6 fields/cell line) showing GFP+ cells/cell clusters in the lungs (green dots) 2 h after i.v. injection of KPC and KPCZ tumour cells and control lungs. Scale bar, 500 µm. **(b)** No. of tumours after subcutaneous injection of the indicated cell numbers for the KPC and KPCZ tumour cell lines and calculated fraction of tumourigenic cells. inf =infinite, Chi-square test. **(c)** Representative images showing spheres of KPC and KPCZ tumour cells. Scale bar, 500 µm and 50 µm for higher magnifications. **(d)** Percentage of cells in KPC and KPCZ lines positive for the indicated markers or marker combinations; n=2 biologically independent experiments, error bars show ±S.D. Source data see Supplementary Table 5, Statistics Source Data. Relative mRNA expression levels (qRT-PCR) of indicated genes, mRNA levels of KPC661 was set to 1; n=3 biologically independent experiments, Mann-Whitney test (two-tailed), *p<0.05, **p<0.01, error bars show mean ±S.E.M.

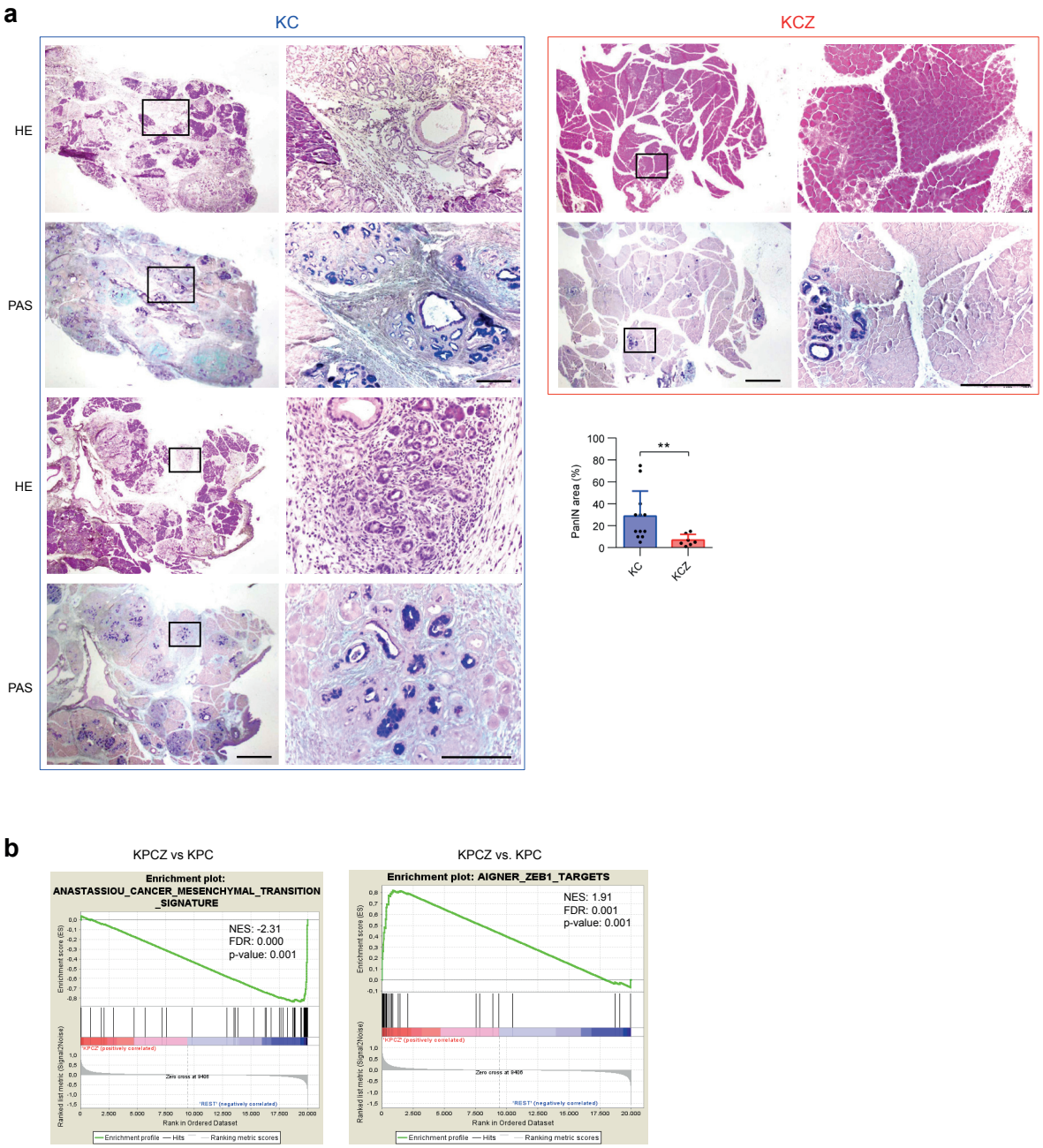

Supplementary Figure 6 Depletion of *Zeb1* reduces early PanIN lesions. **(a)** Consecutive sections showing representative HE and PAS stainings of precancerous PanIN lesions in the pancreas of two different 6 month old KC and of one KCZ mice. Specific dark blue PAS staining indicates the mucin-rich PanIN lesions. Scale bars, 2.5 mm and 150 µm for higher magnifications. Quantification of the PanIN area (% of pancreas area).n=12 KC and 7 KCZ independent mice , error bars show mean ±S.D.; **p<0.01, unpaired Student's t-test (two tailed) with Welch's correction. **(b)** Gene set enrichment analyses (GSEA) of transcriptome data from KPCZ vs. KPC cells reveals reduction of gene signatures associated with cancer mesenchymal transition and Zeb1 targets in KPCZ vs. KPC cell lines. NES = normalized enrichment score; FDR=false discovery rate.

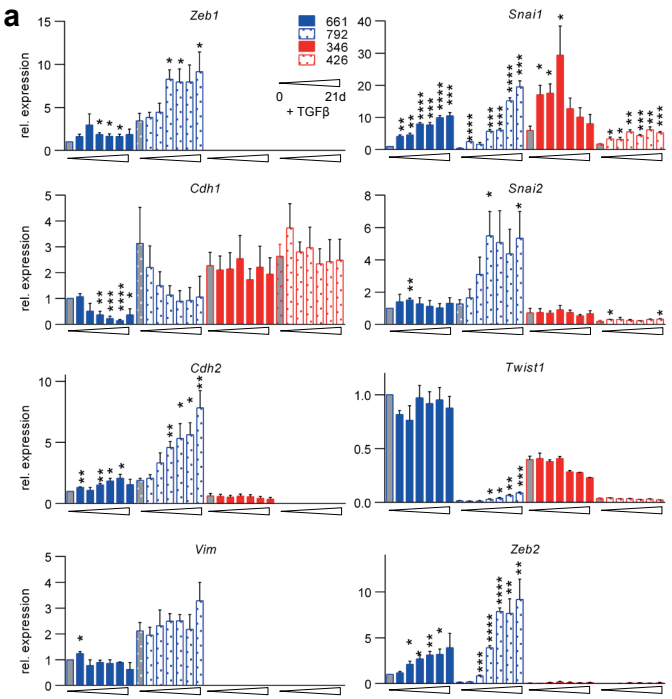

b

log2FC	661+TGFβ vs 661	792+TGFβ vs. 792	346+TGFβ vs 346	426+TGFβ vs 426
Dusp1	1.2*	3.3*	-0.3	-0.2
Lhfp	1.5*	1.9*	-1.0	-0.8
Ddah1	1.7*	1.8*	0.3	-0.1
Thbs1	1.2	1.5*	0.6	-0.1
Ctgf	1.4*	1.1*	0.2	0.1
Cyr61	1.2	1.2	-0.5	-0.3
Flna	0.5	0.5	-0.1	-0.3

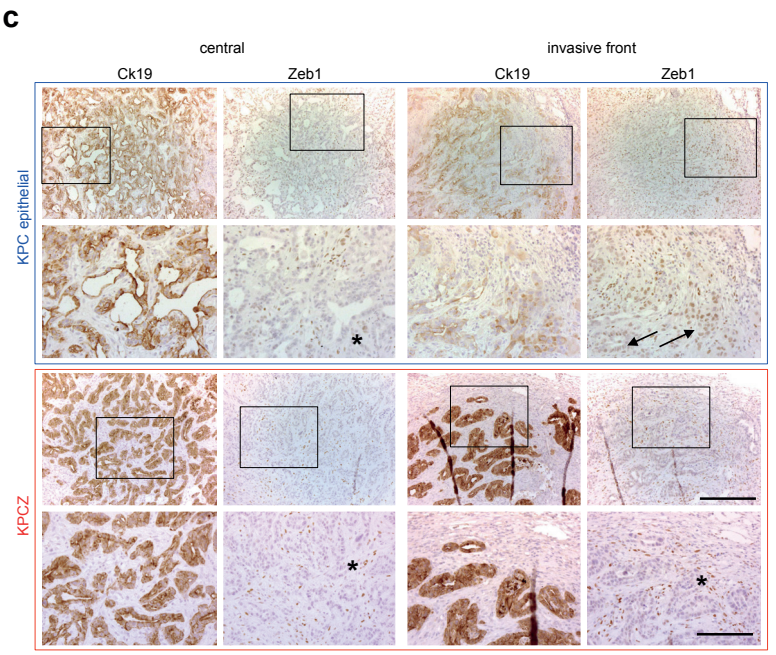

Supplementary Figure 7 Depletion of *Zeb1* reduces tumour cell plasticity. **(a)** Relative mRNA expression levels (qRT-PCR) of indicated genes in KPC and KPCZ cell lines treated for different times with TGFβ (time points: 0, 6 h, 1, 3, 7, 14, 21 days). mRNA levels of cell line 661 at day 0 were set to 1. n=3 biologically independent experiments, error bars show mean ±S.E.M. Statistical analysis is shown for the comparison of TGFβ treated to untreated samples (grey bars) of each individual cell line *p<0.05, **p<0.01, ***p<0.001, ****p<0.0001, unpaired Student's t-test (one-tailed) Source data see Supplementary Table 5, Statistics Source Data. **(b)** Table showing log2FC in mRNA expression levels (microarray) of genes previously determined as common ZEB1/YAP targets in KPC and KPCZ cell lines upon TGFβ treatment for 14 days. (cut-off: adj. p-value<0.05 and log_2FC>0.5). **(c)** Representative images of consecutive sections of immunohistochemistry for Ck19 and Zeb1 comparing the plasticity of Zeb1 expression in central and invasive tumour regions. Tumours derived from one KPC and one KPCZ cell line are shown. Asterisks label Zeb1 expression in stroma cells, arrows indicate Zeb1 expression in tumour cells at the invasive front. Ck19 expression is shown to identify cancer cells. n= 15 KPC, 13 KPCZ independent tumours, Scale bars, 50 μm and 150 μm for higher magnifications.

Fig. 2d

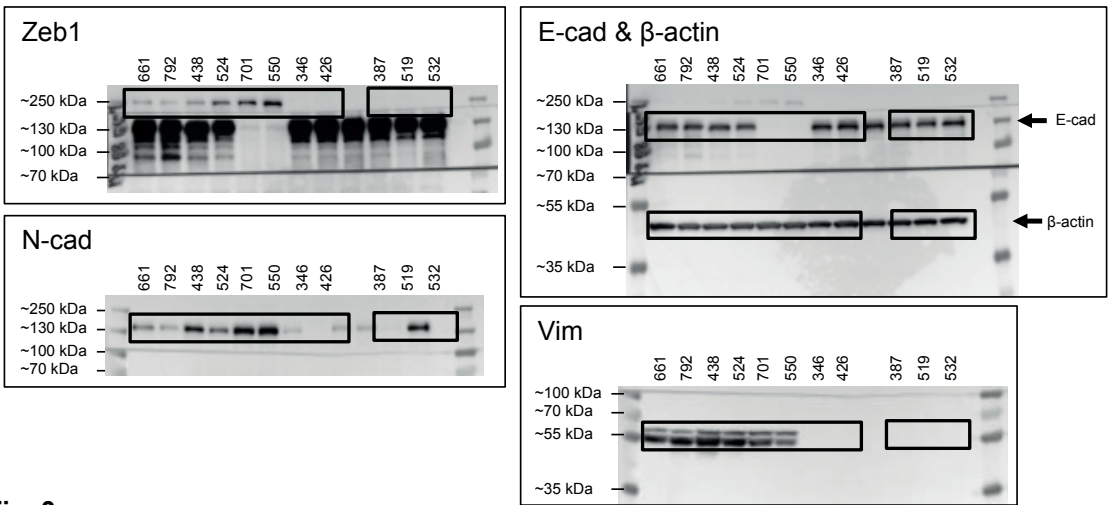

Fig. 3c

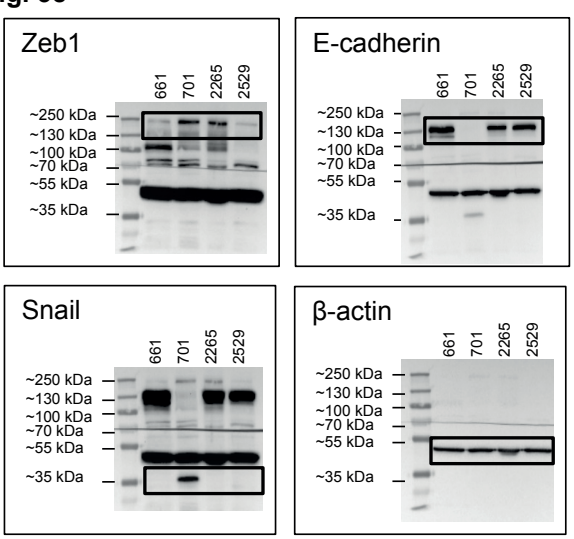

Fig. 3d

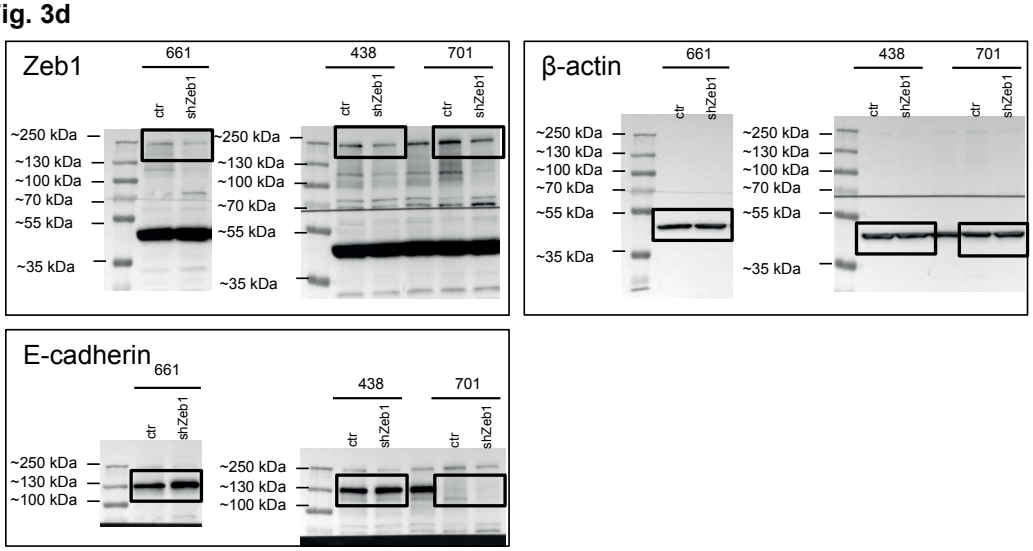

Supplementary Figure 8 Unprocessed scans of immunoblots

Fig. 3f

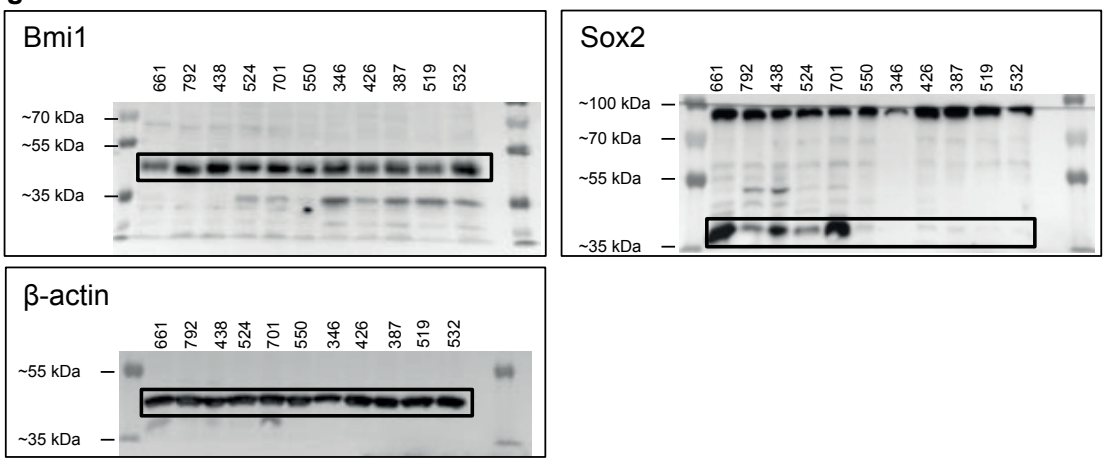

Fig. 3h

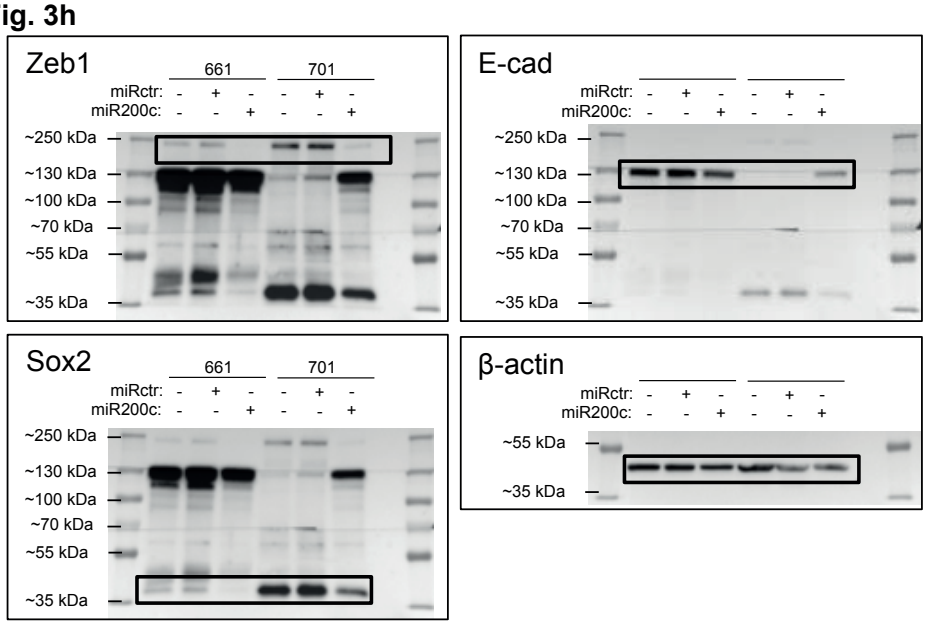

Fig. 5c

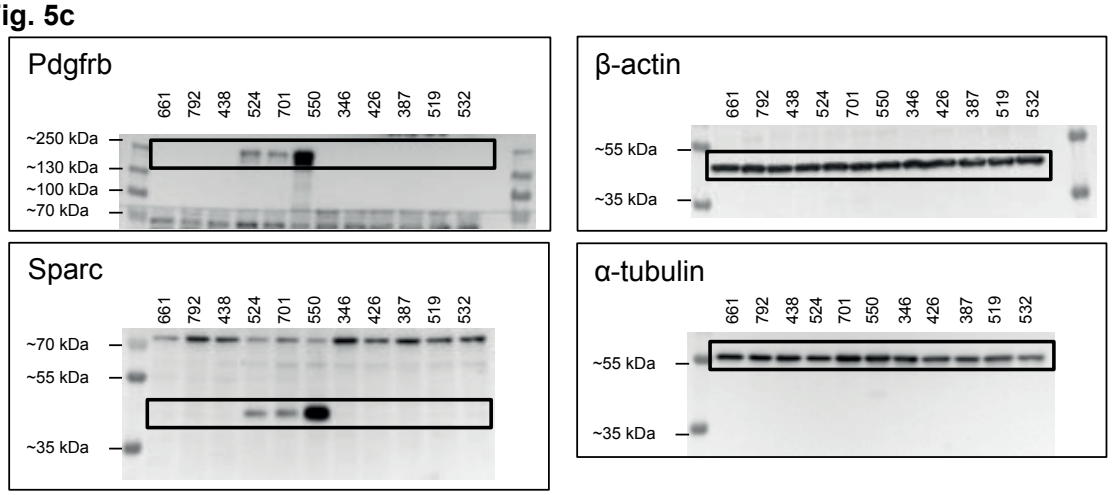

Supplementary Figure 8 Continued

Fig. 6b

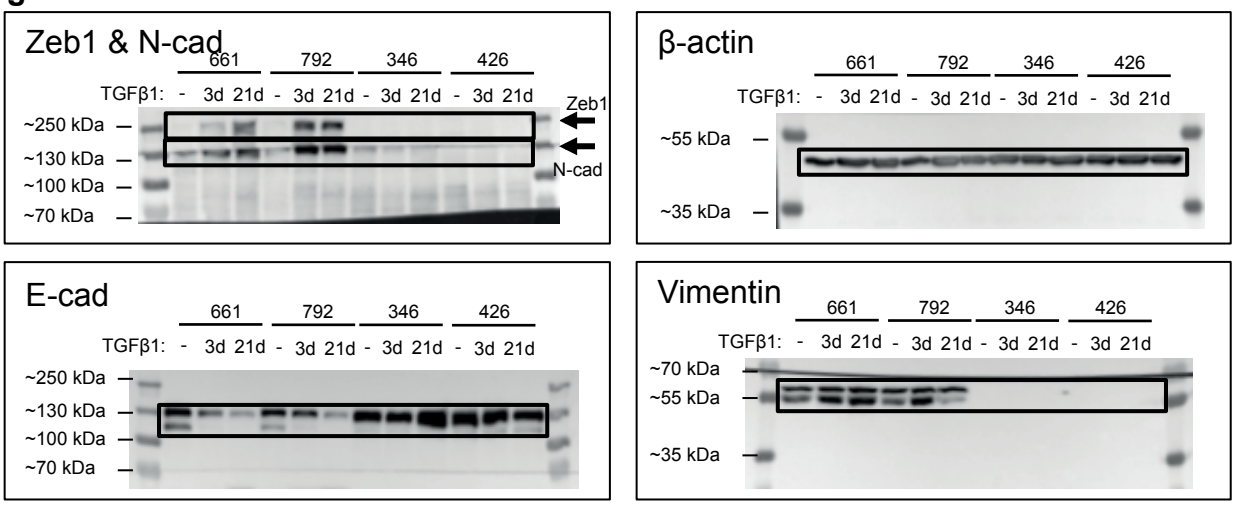

Fig. 6f

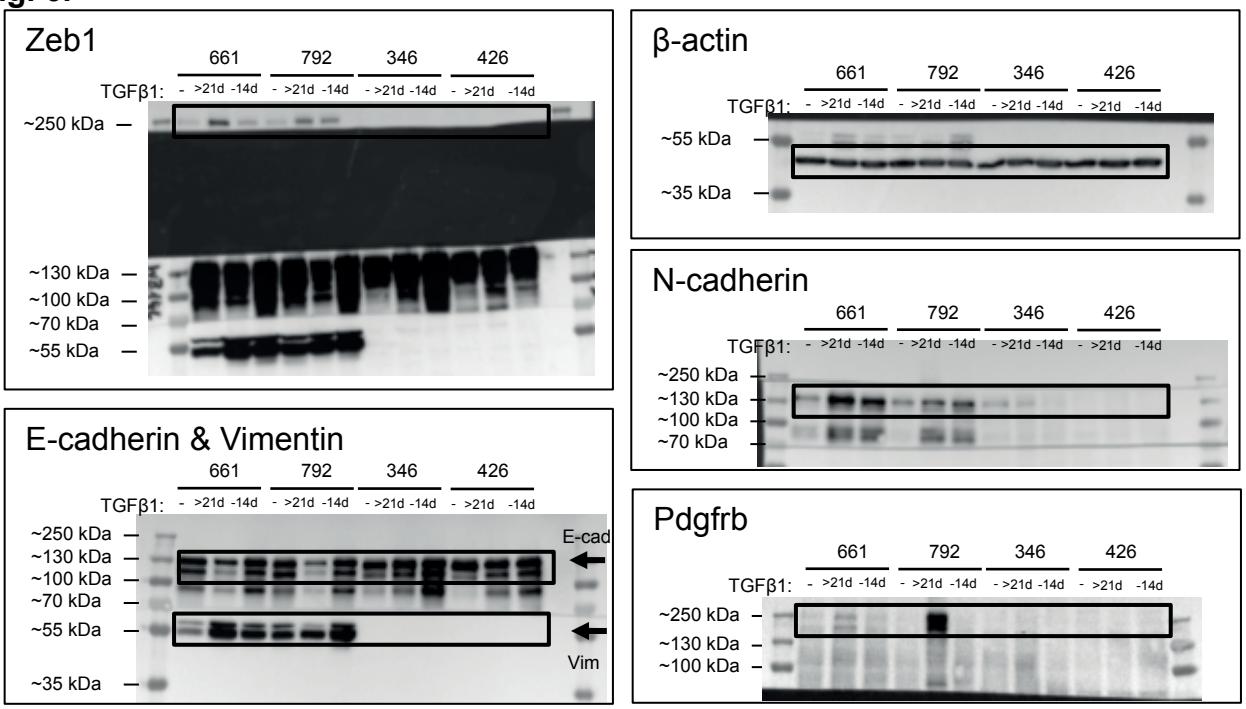

Supplementary Figure 8 Continued

Supplementary Table Legends

Supplementary Table 1 Overview of all KPC and KPCZ mice included in the study

Supplementary Table 2 Genes up- or downregulated upon long-term TGFβ treatment in epithelial KPC and KPCZ cells

Supplementary Table 3 Information on primers used for qRT-PCR

Supplementary Table 4 Selected 36 gene sets used for gene set enrichment analysis. Names and online link for the 36 publically available gene sets used for gene set enrichment analysis related to pancreatic cancer, Zeb1 or metastasis.

Supplementary Table 5 Statistics Source Data